

Discovering hidden layers in quantum graphs

Lukasz G. Gajewski* and Julian Sienkiewicz

Faculty of Physics, Warsaw University of Technology, Koszykowa 75, 00-662 Warszawa, Poland

Janusz A. Hołyst

*Faculty of Physics, Warsaw University of Technology, Koszykowa 75, 00-662 Warszawa, Poland and
ITMO University, Kronverkskiy Prospekt 49, St Petersburg, Russia 197101*

Finding hidden layers in complex networks is an important and a non-trivial problem in modern science. We explore the framework of quantum graphs to determine whether concealed parts of a multi-layer system exist and if so then what is their extent, i.e., how many unknown layers there are. Assuming that all information available is the time evolution of a wave propagation on a single layer of a network it is indeed possible to uncover that which is hidden by merely observing the dynamics. We present evidence on both synthetic and real-world networks that the frequency spectrum of the wave dynamics can express distinct features in the form of additional frequency peaks. These peaks exhibit dependence on the number of layers taking part in the propagation and thus allowing for the extraction of said number. We show that in fact, with sufficient observation time, one can fully reconstruct the row-normalised adjacency matrix spectrum. We compare our propositions to a machine learning approach using a modified, for the purposes of multi-layer systems, wave packet signature method.

I. INTRODUCTION

A plethora of contemporary dynamical systems and collective phenomena can be expressed in terms of complex networks and recently often with multi-layer models. Whether it is a transportation network (e.g., buses and trams) or a social one (e.g., Twitter and Facebook) various forms of information propagation or state dynamics can be described with multi-layer networks. [1–7]

However, it is not uncommon for certain parts of a system to remain hidden from observers and it can be crucial to be able to discern what characteristics are unknown and then to try to obtain them. Such inverse problems have been studied in various settings in both topology and dynamics parameters reconstruction in mono- and multi-layer scenarios alike [8–20]. Recently there have been some pivotal advances in terms of determining whether one can detect hidden layers in non-markovian dynamics and even obtain how many of these layers are there [21].

Nevertheless, to our knowledge, there has not been much done specifically for uncovering the multi-layer structures in quantum graphs and thus we address this issue and present two potentially viable approaches of establishing if hidden layers exist and in some scenarios to ascertain the exact count of these layers.

Traditionally graphs are discrete, combinatorial abstract mathematical objects. If we supply them with a metric and topology we call such objects *metric graphs*. Those in turn equipped with a second order differential operator acting on its vertices and edges - a Hamiltonian - and appropriate boundary conditions are called *quantum graphs* [22–25]. It is worth underlining here

that with this definition we do not specify the exact nature of the Hamiltonian and while it is often a quantum mechanical one it need not be so and thus here we follow the interpretation of taut strings, fused together at the vertices that can be seen as the “limiting case” of a “quantum wire” [26, 27]. The (most likely) first use of this framework can be traced back to Pauling’s paper in 1936 [28], however, for the most part quantum graphs have not been widely used until more recently. Nowadays they see many various applications in dynamical systems, nanotechnology, photonic crystals and many others [29–34]. Most recently Aziz *et al.* established a method based on a wave packet propagation on quantum graphs that allows to distinguish between structures in complex networks [35] thanks to many well studied properties of the Laplacian (e.g., finite speed of propagation [36] as opposed to a discrete Laplacian [37, 38]) and its spectra in quantum graphs [39–45]. The idea of determining the a shape of an object based on observable dynamics on it goes back to the work of Kac in 1966 [46] in which he asks whether it is possible to hear the shape of a drum. Giraud and Thas showed that the eigenvalues of different shapes can be identical and therefore answered Kac’s question in the negative. Gutkin and Smilansky, on the other hand, showed that in quantum graphs specifically, under certain conditions, one can indeed “hear” the shape as the Hamiltonian uniquely defines the connections and their lengths when the graph is finite (and simple), the bond lengths are rationally independent and the vertex scattering matrices are properly connecting. It is also worth noting that this inverse spectral problem can be extended onto scattering systems as also stated in the same paper (a so called inverse scattering problem [47]). However, in appears it is *not* always possible [48, 49] (i.e., there is a way to construct iso-scattering pairs of graphs with identical polar structure of their scattering matrices) which was also showed experimentally via microwave networks

* lukaszgajewski@tuta.io

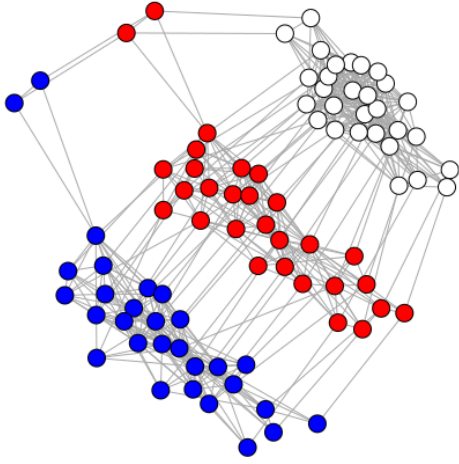


FIG. 1. Three-layered multiplex representation of the Vickers [54] data.

by Hul *et al.* [50]. Wave packets specifically have also attracted some attention in recent years but not for the purposes of the goal we aim for in this paper [51, 52]. Some work has been done in context of sufficient coverage with sensors [53], however, in this case we also will not share all the assumptions and thus those methods are not applicable to our problem.

In this paper we tackle the problem of determining whether there are hidden layers in the complex system we are observing and if so then how many. We assume a wave packet propagation dynamics on a quantum graph as our model for the dynamical system. Each edge e in the graph G has an associated length $l_e = 1$ and a spatial coordinate variable $x_e \in [0, l_e]$ along said edge. We use a special case of a Hamiltonian - an edge based Laplacian giving us an edge-based wave equation on a graph in the form:

$$u_{tt}d\mathcal{E} = -\Delta u \quad (1)$$

where \mathcal{E} is a Lebesgue measure on the graph's edges [26, 55].

We use Neumann boundary conditions stating that the sum of outward pointing gradients at every vertex must vanish [26, 35]:

$$\forall v \in G, \sum_{e \ni v} (-1)^{1-x_{e,v}} \nabla f(e, x_{e,v}) = 0 \quad (2)$$

The initial condition for the wave equation is Gaussian wave packet:

$$f(e, x) = \exp(-a(x - \mu)^2) \quad (3)$$

which is fully contained within a single edge with the highest betweenness centrality [56] following the conventions of Aziz *et al.* [35]. We simulate many layer system in a multiplex configuration, i.e. each node is connected to its reflection in a neighbouring layer (see Fig. 1 for a

real-world network example and Fig. 2 for wave propagation example on a simple synthetic graph). While the propagation simulations are computed on full systems, for the detection purposes we always only use information from a single layer, i.e., all but one layer are hidden from the perspective of our methods at all times.

This rest of the paper consists of three main parts followed by a discussion. Firstly we briefly outline the approach introduced by Aziz *et al.* in [35] and show its viability for the purposes of multi-layer networks in the context described above. Secondly we introduce our own approach with the use of a Fourier transform on the time evolution of sum of amplitudes in the visible part of the system. Thirdly, we show that with sufficient resources (i.e., observation time) one can fully reconstruct the spectrum of the row-normalised adjacency matrix.

II. GAUSSIAN WAVE PACKET SIGNATURE (WPS)

Gaussian wave packet signature (WPS) is a methodology developed by Aziz *et al.* [35] that allows to distinguish between various types of graphs. The procedure starts by initiating an edge with a Gaussian wave packet that is completely contained on said edge (see Fig. 2a). The edge is chosen to be the one with the highest betweenness centrality as to assure the fastest possible spread of the wave on the graph (although this can, of course, be relaxed in general). Then on each integer time we measure the amplitude in the centre of every edge $2|E|$ times in total, where $|E|$ is the number of edges (see Fig. 2b and Appendix A for a detailed description of the way the amplitude is calculated). We measure the centre of each edge because at integer times the highest value is in the centre. Finally, we create a histogram with 100 bins of these measurements - this is the WPS of the graph. Aziz *et al.* show that particular graph types (say Barabási-Albert, Erdős-Rényi, etc.) will have similar WPSs yet different in comparison to other types (so, e.g., one can differentiate an ER from a BA). In order to actually do this differentiation one must build a classifier. In their work a K-nearest neighbours (K-NN) classifier was chosen. From the perspective of the machine learning tools we use in this paper (K-NN, PCA) each histogram bin of the WPS is a dimension in the feature space.

For our purposes we will deviate slightly from this procedure. Namely to us the whole graph is not known and the graph itself is a multiplex. Additionally, we assume that the wave propagation is an actual process ongoing through some network. Thus, we assume we have access to a single layer on which a certain spread has happened that can be modelled with a Gaussian wave packet and we suspect there may be hidden layers in the network. Question is - can we detect their presence?

The rest of the procedure is similar, i.e., we create a WPS and we train a classifier on a given type of a graph

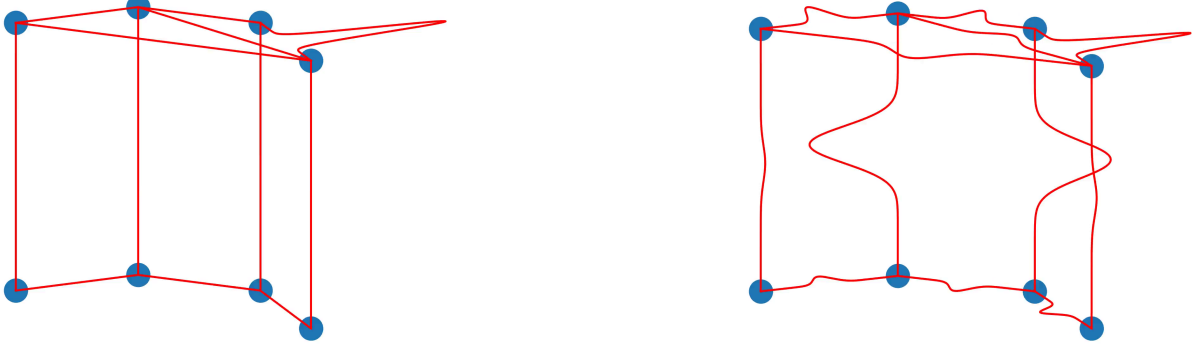


FIG. 2. An exemplary picture of a wave starting at a specific edge (left, $t = 0$) and then propagating through the multiplex system (right, $t > 0$).

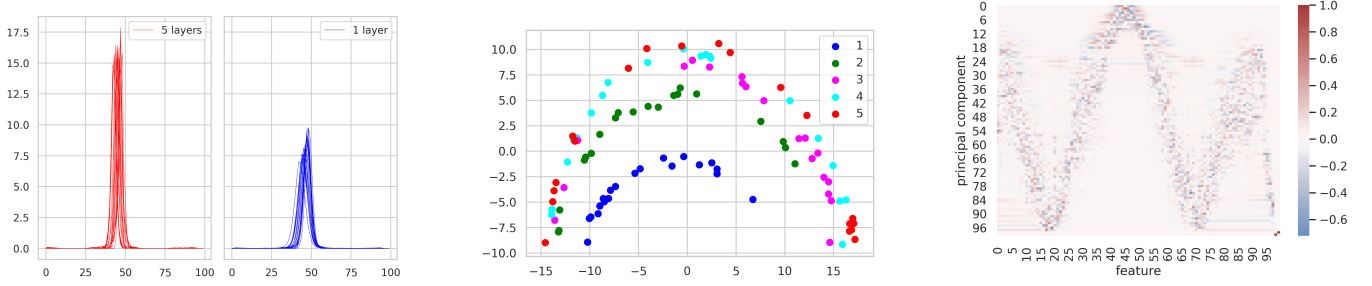


FIG. 3. Wave packet signatures (left) for various realisations of a Barabási-Albert ($N = 50$, $m = 3$) graph with 5 and 1 layers (measured on one layer only). WPS projected onto a 2D space with PCA (centre) with colours distinguishing no. of layers. Each point is a different BA graph. PCA transformation matrix (right) showing the contributions of given WPS bins into principal components.

(e.g., BA) and this time the classes are the number of layers. See Figs 3 and 4 where we compare WPSs of a 5-layer BA graph vs 1-layer and a 5-layer ER graph vs 1-layer respectively. One can clearly see that the signatures are distinct. To further illustrate this we use Principal Component Analysis (PCA, see Appendix B for details) to project the WPSs onto a 2D space (see the centre pieces of Figs 3, 4). There one can see that each class takes a distinct region of space and thus we should be able to discriminate between them. However, it is worth noting that the more layers there are the more tightly packed the observations are, i.e., discriminating between mono-layer and penta-layer graphs is fairly easy, between tetra- and penta- not as much. It is also worth noting that through PCA we can see that the centre bins carry the most variance in the feature space (see panels on the right in Fig. 3, 4) and that there are certain distinct structures visible in the higher PCs for both BA and ER graphs.

As mentioned before, we follow Aziz *et al.* and also choose the K-NN for classification (see Appendix C for a description of the K-NN method). We build the model on various graphs with between 1 to 5 layers (with val-

ues only from one layer each time as explained earlier) and then test it to see if it can recognise how many layers there are in an unknown graph. We conducted our tests for BA and ER graphs (see Fig. 5 for results of classification). For each type of graph we simulated 500 independent realisations (100 per each number of layers) with mean degree $\langle k \rangle = 6$ and network size $N = 50$. We take out a 100 randomly chosen, in a stratified manner (i.e., classes are equally represented), realisations out of the data set (this will be the test set). On the training set we conduct 100 rounds of training and then testing. That is in each round we do the training/test split, then a 10-fold cross-validation on the training set to find the best K parameter of the K-NN model and then use that on the test set. We present the results in a form of box plots. In Fig. 5 we show the accuracy of the classifier for both BA and ER. We can see that while for ER the results are slightly lower than for BA, in both cases the accuracy is still fairly high with medians of 92 and 89 for BA and ER respectively.

To additionally illustrate the point made earlier that higher numbers of layers are more difficult to discern amongst one another we show the diagonal values of con-

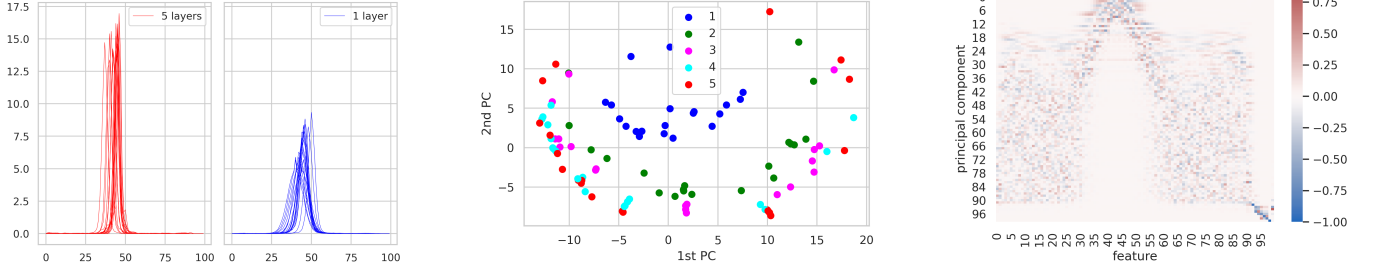


FIG. 4. Wave packet signatures (left) for various realisations of a Erdős-Rényi ($N = 50$, $\langle k \rangle = 6$) graph with 5 and 1 layers (measured on one layer only). WPS projected onto a 2D space with PCA (centre) with colours distinguishing no. of layers. Each point is a different ER graph. PCA transformation matrix (right) showing the contributions of given WPS bins into principal components.

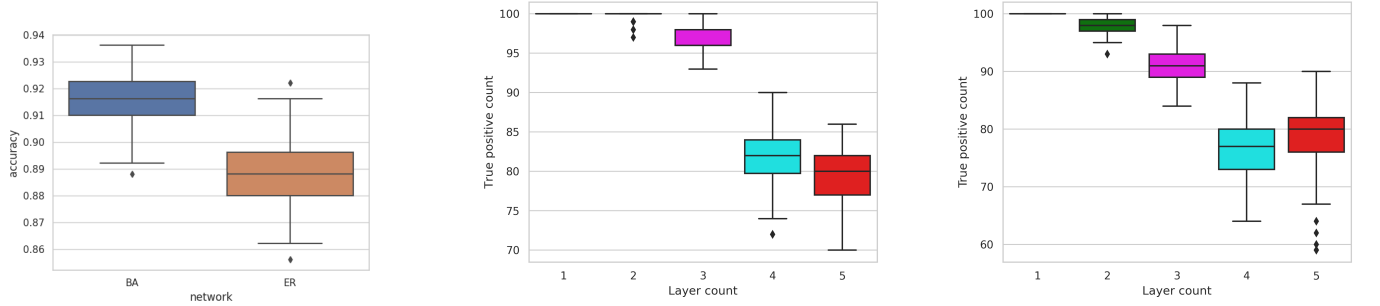


FIG. 5. K-nearest neighbours classification accuracy of the layer count for a BA and ER graph as box plots (left) based on single layer WPSs. Contingency table diagonal values as box plots for a BA (centre) and ER (right). We simulated 400 independent realisations of a given graph type (BA, $N = 50$, $m = 3$; ER, $N = 50$, $\langle k \rangle = 6$). For each type of graph we conducted 100 rounds of 10-fold cross-validation to determine the K parameter in K-NN withdrawing 100 realisations (25%) for purposes of final evaluation. Train/test split was random and stratified.

tingency tables from all 100 rounds for BA (centre panel of Fig. 5) and ER (the right panel of Fig. 5). One can clearly see that identifying mono-layer systems is practically 100% accurate and it is the more layered systems that cause trouble for the classifier.

While the classification results seem very promising it is important to note the obvious and major disadvantage of this approach. One must build a training set for it to work. With synthetic networks it is easy to generate as many as one wants and the limitation is purely computing power. When dealing with real-world networks one often does not simply have the ability to have similar enough graphs to the one currently under observation but with added layers. In such a circumstance perhaps a combination of many different synthetic networks could suffice and other, more advanced, classification methods than K-NN could be utilised. That, however, is beyond the scope of this study.

III. FOURIER TRANSFORM OF THE AMPLITUDE SIGNAL

Here we introduce a new approach to detecting layers on quantum graphs. Similarly to the previous case we

assume we can either produce or observe a wave propagation on the graph initiated by a Gaussian wave packet. For efficiency's sake in the simulations used we used the edge with the highest betweenness centrality as before and we also measure the amplitudes at integer times in the centres of all edges for $2|E|$ times. While in WPS method we simply follow the advice of Aziz *et al.* for the count of measurements in the approach discussed here it is usually rather clear if enough data was collected by straight forward visual inspection.

Our proposition is as follows, at each integer time compute the sum of all amplitudes in the visible part of the system and treat it as a time dependent signal $S(t)$. Transform the signal into frequency domain via a fast Fourier transform (see Appendix D and [57]) - $\hat{S}(f)$ - and look at the spectrum of the signal - $|\hat{S}(f)|^2$.

A mono-layer system will produce a “flat” signal $S(t)$ whilst multi-layer one will exhibit periodic behaviours due to energy leaking in and out of the visible layer from and into other layers. At sufficiently long measurement time scale the signal should stabilise and become stationary as long as no perturbation is introduced to the overall network. This transfer of energy induces oscillations in the amplitude sum on the visible layer which in turn create clear peaks in the power spectrum, see Fig. 6 for

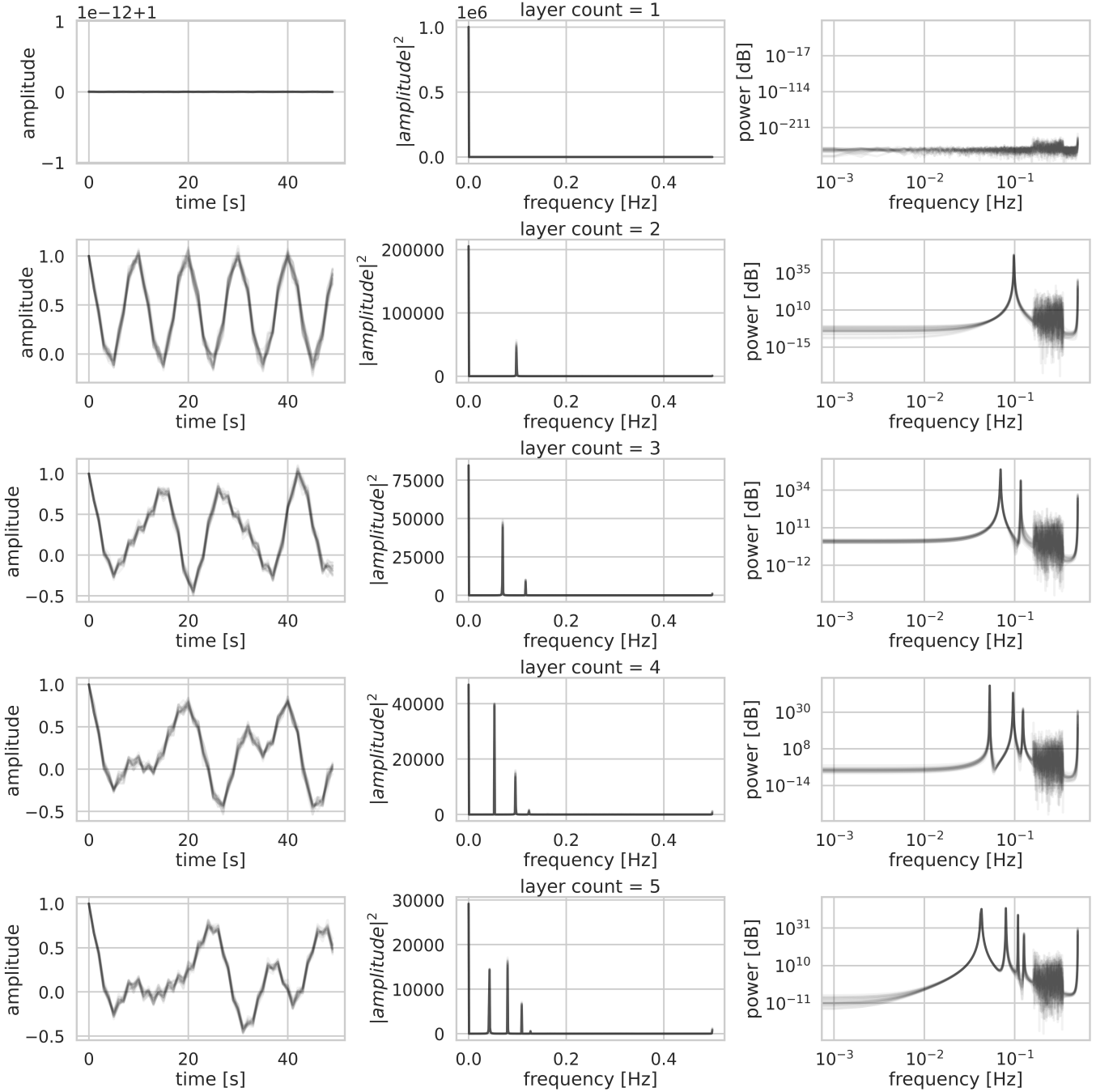


FIG. 6. Sum of amplitudes time evolution as measured on the only visible layer (left). Fast Fourier transform of this signal (centre) and its power spectrum (right). Each row represents a different number of layers (1 to 5 going top to bottom). Simulations conducted on 20 independent realisations of a BA graph ($N = 50$, $m = 3$) per row, overlaid with transparency. Note: for the purposes of the Fourier analysis we use signals of length 10^3 s.

results from BA graphs (and Fig. 13 for ER, presented in Appendix H). Left column shows the signal $S(t)$, centre $|\hat{S}(f)|^2$ and right $|\hat{S}(f)|^2$ in decibels and log-log scale. Each row has 20 independent realisations plotted on top of each other with transparency to show that these peaks are fairly consistent, and different number of layers (1st row are mono-layer systems, 2nd row bi-layer, etc.). It

is quite apparent that there are visible peaks and their count strictly corresponds to the number of layers in the system.

These results already show the advantage of FFT over WPS as it is simpler and does not seem to suffer from struggling to differentiate as much between high-layer systems. Additionally it does not require any prior

knowledge or learning of the model. It is far from flawless, however. As it is much easier to test on real networks than WPS we applied it to three real-world networks [54, 58, 59] - see descriptions in Appendix E. The results are in Fig. 7 where one can see that while we do get peaks in the spectrum and therefore can confidently state that there are hidden layers, it is much less clear how many of them there are. This is most likely due to the fact that these networks are not as clear cut multiplexes as the synthetic systems we discussed earlier. These networks here have various mean degrees in each layer and that also implies varied coupling strength between the layers. Additionally real-world networks can have other characteristics different between the layers such as clustering coefficients or degree distributions and the synthetic systems tested simply do not have this property. However, we show in the next section that it is possible to reconstruct the full spectrum of the row-normalised adjacency matrix with this method and therefore determine the number of layers for any system.

IV. SPECTRUM RECONSTRUCTION

In this section we show that with sufficiently long observation it is possible to completely recover all eigenvalues of row-normalised adjacency matrix of the full system and thus trivially determine the number of hidden layers.

We shift slightly from previous sections as we no longer take measurements on the edges but only on nodes. This makes the problem less computationally intensive and also, in our opinion, makes for a more practical case as it might be sometimes easier to observe just the nodes' states (see Appendix A for details). However, same analysis can be applied using edge measurements as previous sections could be done with node values only - we chose otherwise as we are stemming from the work of Aziz *et al.*

Similarly as before we observe the sum of amplitudes, however, in this case it is important to have enough samples of the signal to provide sufficient resolution in the power spectrum. How long one needs to observe a system will of course depend on the intricacies (and mostly size) of the system in question. As the propagation process is not stochastic the time needed for observation is finite and in our experience not unattainable. The goal is simply to have the complete power spectrum of the signal. Then one takes note of the peaks present - we opted for an automated approach using a wavelet transform [60] (see Appendix F). These peaks in the power spectrum correspond to the eigenvalues of the Hamiltonian (divided by 2π) which in turn directly relate to the eigenvalues of the row-normalised adjacency matrix - $\hat{\mathbf{A}}$ - such that each eigenvalue $\lambda \notin \{-1, 1\}$ of $\hat{\mathbf{A}}$ has corresponding Hamiltonian eigenvalues $\arccos(\lambda)$ and $2\pi - \arccos(\lambda)$. This leads us to two important results, (i) the number of frequencies present in the power spectrum $\#f$ is two less than count of eigenvalues of the adjacency matrix and

since we know the layer sizes (i.e., node count per layer - N) as a multiplex structure was assumed the number of layers $K = (\#f + 2)/N$; (ii) we can in fact recover almost exactly all eigenvalues of $\hat{\mathbf{A}}$ as $\cos(2\pi f_i)$ for each frequency peak f_i in the power spectrum.

We present the result of the full spectrum reconstruction on Fig. 8 for a complete, BA and real-world graph. We chose the complete graph as it has a special case due to the extreme symmetries of the multiplex adjacency matrix and thus the number of peaks directly corresponds to the number of layers unlike more complex cases where the eigenvalues multiplicities behave differently. Of course, this does imply that if due to specific structures in a given system some eigenvalues have high multiplicity the simple formula $K = (\#f + 2)/N$ will not hold and system specific adjustments would be needed. The reconstructed eigenvalues give an almost perfect match with those of the row-normalised adjacency matrix. Note that the performance here is mostly limited by the peak detection method and the resolution in the frequency domain, i.e., the information is there in the spectrum, the only challenge is to recover it efficiently.

In order to explicitly show the correspondence between the eigenvalues of the Hamiltonian and the peaks of the power spectrum we follow in detail the full graph case, considering the simplest configurations - a monoplex and a duplex network (see Appendix G). Our exact analytical solutions prove that for the duplex network of N nodes on each layer, among $2N$ eigenvalues that characterise the system we have only four distinct ones $\lambda = \{-\frac{2}{N}, 0, \frac{N-2}{N}, 1\}$, the first two having multiplicity of $N-1$. Figure 9 shows that in such a system one recovers just one eigenvalue, i.e., $\lambda = \frac{N-2}{N}$ directly connected to periodicity of the sum of observed amplitudes on nodes. On the other hand, observing a single node allows for the recovery of the full spectrum (see Appendix G and Fig. 12 for details).

V. DISCUSSION

In this paper we explore the paradigm of quantum graphs as a potential tool for studying multi-layer networks. The particular problem we are interested in is determining whether there are hidden layers of communication in the system that we cannot observe by taking measurements of the ongoing dynamics in the single layer that we can observe. We proposed and tested two methods - one based upon a Gaussian wave packet signature (WPS) that was introduced prior by Aziz *et al.* to discriminate between various types of mono-layer systems and the other on observing the power spectrum of the wave amplitudes.

WPS is a method where a Gaussian wave packet, either observed or purposefully produced, initiates the propagation from a single edge and we take measurements of amplitudes at every edge at integer times sufficiently long. Such data is then histogrammed to produce the signa-

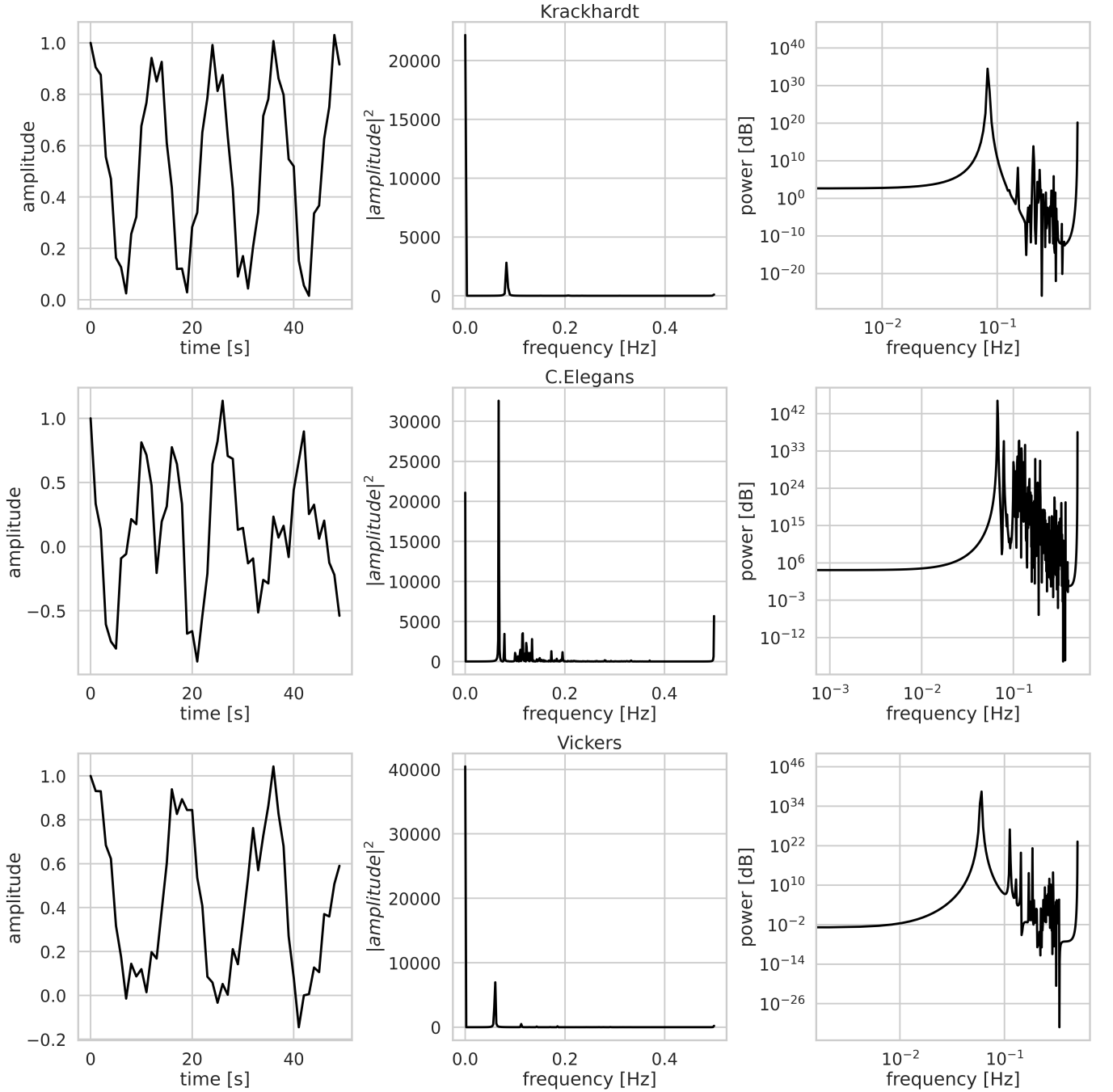


FIG. 7. Sum of amplitudes time evolution as measured on the only visible layer (left). Fast Fourier transform of this signal (centre) and its power spectrum (right). Each row represents a different real-world network (as indicated by titles - Vickers[54], C.Elegans[59], Krackhardt[58]). Each graph is a 3-layered multiplex. Note: for the purposes of the Fourier analysis we use signals of length 10^3 s.

ture. This signature has the property of being similar within a category of graphs while varied without. That is, e.g., signatures of ER graphs are similar to one another but different from BA graphs, or for our purposes, mono-layer graphs have different signatures than multi-layer ones etc. This in turn can be utilised by machine learning models, such as K-nearest neighbours, to build

a model capable of discriminating between graphs with different number of layers. This approach suffers from several issues. Most prominently it requires a training sample. This can be very difficult to obtain in real-world scenarios and while perhaps a well varied synthetic data set could suffice at this point it is a mere speculation. The choice of appropriate machine learning scheme and

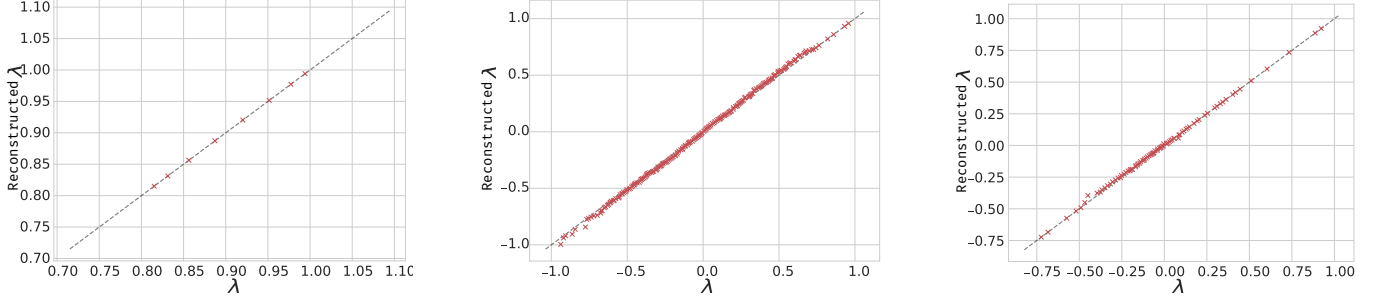


FIG. 8. Eigenvalues reconstruction from the Fourier spectrum of the nodes' amplitudes sum signal. (Left) an example of a complete graph multiplex with layer size $N = 20$ and number of layers $K = 9$. As it is a special case of an extremely symmetric adjacency matrix there are only as many eigenvalues as there are layers. (Centre) a Barabási-Albert graph with $N = 50$, $m = 3$, $K = 4$ has a much more complex spectrum and so does a real-world network (right) - Vickers[54] - both of which we attain an almost perfect match between the recovered and actual eigenvalues. The dashed diagonal line is a visual aid showing “ $y = x$ ”.

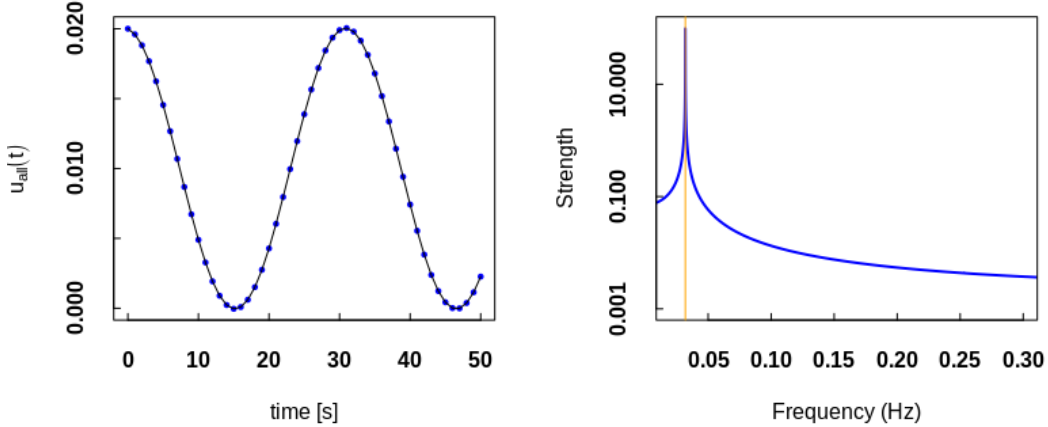


FIG. 9. Full graph duplex with $N = 100$ nodes in each layer: (a) Sum of amplitudes over time in a single layer; lines are guidance to eye connecting theoretical predictions from Eq. (G29) that are exactly covered with points obtained from numerical simulations, (b) Power spectrum of the signal shown in panel (a) [the series consists of 10000 elements]. Vertical line is frequency equal to $\omega_{2N-1}/2\pi = (N - 2)/(2\pi N)$.

its construction is also a non-trivial task. Additionally as the number of layers grows differentiating between such networks becomes increasingly difficult since the signatures become less varied.

We also introduce an approach that utilises a discrete Fourier transform (DFT) instead of a machine learning model. Instead of histogramming the measurements as before, one computes the sum of the amplitudes on the visible layer at each integer time. This constitutes a signal that at sufficient time scales should become stationary. In a mono-layer system the signal will simply be a constant value due to energy conservation. However, should other layers be in the system from the perspective of the mono-layer there will be oscillations as the energy will flow out and back into it. We can inspect those oscillations with the use of DFT and look at the

power spectrum. The spectrum will exhibit characteristic peaks absent in mono-layer networks. The number of these peaks strictly corresponds with the number of layers in the synthetic scenarios tested. This approach is significantly advantageous over the WPS as it does not require building a learning sample and is in general much simpler. Furthermore it does not really suffer in terms of differentiating, e.g., tetra- from penta-layer systems, etc. Although it shows much promise in synthetic scenarios, it does not perform as well in real-world networks. It does indeed indicate clearly that there are hidden layers but the number of them can be rather tricky to discern. This is perhaps not that surprising considering that real-world networks are much more “messy” in some way than synthetic examples. Layers vary in size, degree distribution, clustering coefficients and so on and so forth while say a

penta-layer BA graph shares all characteristics between layers even though the exact connections are different. Those and other features of real-world systems could also affect the coupling amongst the layers that most certainly will affect the nature of the amplitude signal.

In such cases (i.e., where peak count after a brief observation is not enough) we show that simply a longer observation time is required. As the signal is not stochastic and oscillation periods is finite it does not seem unfeasible to observe enough of the signal to determine its power spectrum with sufficient resolution. Then each peak in the spectrum corresponds to the Hamiltonian eigenvalues that in turn are related to the eigenvalues of the row-normalised adjacency matrix via simple formula. With this we showed that it is indeed possible to recover all these eigenvalues and thus trivially determine the number of layers in the system.

It is worth underlining here that a row-normalised adjacency matrix is in fact a so called right stochastic matrix of a given graph and while it goes beyond the scope of this paper, there exist methods of reconstructing the whole matrix from its spectrum [61–65] which we suspect should be quite feasible considering we already assume knowing part of it (one layer and inter-layer structure). That in turn could also open the door to the adjacency matrix itself. Recovering all the connections exactly may not be possible, however, having a matrix iso-spectral to the adjacency matrix is also very valuable as having this spectrum allows for determining many important properties of the system [66, 67].

We find that both methods presented in this paper - the WPS and FFT - show enough success in these simple scenarios we tested to merit further study, such as in noisy (or stochastic) systems, for instance. They each have their pros and cons that we hopefully managed to outline clearly as well as the potential room for improvement of their applicability and understanding of waves

on quantum graphs alike.

ACKNOWLEDGMENTS

The project was partially funded (LG) by POB Research Centre Cybersecurity and Data Science of Warsaw University of Technology within the Excellence Initiative Program - Research University (ID-UB). JS acknowledges support by National Science Centre, Poland Grant No. 2015/19/B/ST6/02612 while JAH was partially supported by the Russian Science Foundation, Agreement No 17-71-30029 with co-financing of Bank Saint Petersburg, Russia.

Appendix A: Calculation of the wave amplitude

1. Overall description

The general solution of the wave equation on graph G , provided that the initial condition is Gaussian packet fully localised on a given edge f is derived and presented in detail by Aziz *et al.* in [35]. Here, we re-write it in terms of integer times, i.e., $t = 0, 1, 2, \dots$ so that it fits the case examined in the main text. We additionally assume that the graph is unweighted, undirected and non-bipartite. In such a setting, we consider an arbitrary edge $e = \{u, v\}$ that connects two vertices u and v and can be associated with a variable $x_e \in [0, 1]$ that represents coordinate along such an edge. Then the amplitude u of the wave in the middle of the edge e can be expressed as

$$u(e, f, t) = u_1(e, f, t) + u_5(e, f, t) + \frac{1}{|E|}, \quad (\text{A1})$$

where $|E|$ is the number of edges in the graph and u_1 and u_5 are defined as follows

$$\begin{aligned} u_1(e, f, t) &= \sum_{\omega \in \Omega} C(e, \omega) C(f, \omega) \cos(B(e, \omega) + \tfrac{1}{2}\omega) \cos(B(f, \omega) + \omega(\tfrac{1}{2} + t)) \\ u_5(e, f, t) &= 2 \cos(\pi t) \sum_i C_\pi(e, i) C_\pi(f, i) \end{aligned} \quad (\text{A2})$$

In the above equations ω , $C(e, \omega)$ and $B(e, \omega)$ come from the edge-based eigenvalues and eigenfunctions, which are, respectively ω^2 and $\phi(e, x_e) = \pm C(e, \omega) \cos(B(e, \omega) + \omega x_e)$ of the row-normalised adjacency matrix $\hat{\mathbf{A}}$ of the graph G . Assuming that we know vertex-based eigenvector-eigenvalues pairs $(g(v), \lambda)$ of matrix $\hat{\mathbf{A}}$ we can express $C(e, \omega)$ and $B(e, \omega)$ as

$$\begin{aligned} C(e, \omega)^2 &= \frac{g(v, \omega)^2 + g(u, \omega)^2 - 2g(u, \omega)g(v, \omega) \cos \omega}{\sin^2 \omega} \\ \tan B(e, \omega) &= \frac{g(v, \omega) \cos \omega - g(u, \omega)}{g(v, \omega) \sin \omega}, \end{aligned} \quad (\text{A3})$$

while $\omega = \arccos \lambda$. The sign of $C(e, \omega)$ needs to chosen

in order to match the phase, in practice it can be achieved by calculating $\text{sgn}[g(v)]|C(e, \omega)|$. It is always true that one of the eigenvalues is equal to 1 (consequently, $\omega = 0$): this value is responsible for the constant term $1/E$ in Eq. (A2) so it is not included in further calculations, i.e., it does not belong to Ω set in function u_1 . Although $\phi(e, x_e)$ are orthogonal, they still need to be normalised. To fulfil this condition for each $\omega \in \Omega$ we calculate normalisation factor $\rho(\omega)$

$$\rho(\omega) = \sqrt{\sum_e C(e, \omega)^2 \left[\frac{1}{2} + \frac{\sin(2\omega + 2B(e, \omega)) - \sin(2B(e, \omega))}{4\omega} \right]} \quad (\text{A4})$$

where e runs over all edges in graph G . Then, in order to obtain properly normalised value of $C(e, \omega)$ one needs to divide it by $\rho(\omega)$.

For calculations of C_π one first needs to transform the original undirected graph G into a directed one $D(G)$ by simply replacing each edge $e = \{u, v\}$ with two arcs (u, v) and (v, u) . In the next step we create a structure called oriented line graph (*OLG*), constructed by substituting each arc of $D(G)$ by a vertex (such vertices are connected if the head of one arc meets the tail of another arc). Using the adjacency matrix \mathbf{A}_{olg} of the *OLG* we solve

the eigenproblem $\mathbf{A}_{olg}\mathbf{g}_{olg} = \lambda_{olg}\mathbf{g}_{olg}$ and then restrict ourselves to $\lambda_{olg} = -1$ and corresponding eigenvectors (there should be exactly $|E| - |V|$ linearly independent solutions) that form C_π .

Let us note that if we decide to measure wave amplitude on nodes instead of edges the formula is particularly simple as then

$$u_n(e, f, t) = u_1(e, f, t) + \frac{1}{|E|}, \quad (\text{A5})$$

and

$$u_1(e, f, t) = \sum_{\omega \in \Omega} C(e, \omega)C(f, \omega) \left[\cos \left[\left(t - \frac{1}{2} \right) \omega - B(e, \omega) + B(f, \omega) \right] + \cos \left[\left(t + \frac{3}{2} \right) \omega + B(e, \omega) + B(f, \omega) \right] \right] \quad (\text{A6})$$

It follows that in such a case we do not have to create *OLG* and thus the calculations are both less time and resources consuming.

2. An example

In order to make the above concise description clear, let us follow a very simple example of a graph shown in Fig. 10a. In such case, knowing the adjacency matrix \mathbf{A} where $A_{ij} = 1$ if nodes i and j share a link and $A_{ij} = 0$ otherwise, we can write the row-normalised adjacency matrix $\hat{A}_{ij} = A_{ij} / \sum_k A_{kj}$ as

$$\hat{\mathbf{A}} = \begin{pmatrix} 0 & \frac{1}{3} & \frac{1}{3} & \frac{1}{3} \\ \frac{1}{2} & 0 & 0 & \frac{1}{2} \\ \frac{1}{3} & \frac{1}{3} & 0 & \frac{1}{3} \\ \frac{1}{2} & 0 & \frac{1}{2} & 0 \end{pmatrix}. \quad (\text{A7})$$

Solving the eigenproblem $\hat{\mathbf{A}}\mathbf{g} = \lambda\mathbf{g}$ one obtains in this case the following eigenvectors

$$\mathbf{g} = \begin{matrix} & \omega_1 & \omega_2 & \omega_3 & \omega_4 \\ \begin{matrix} 1 \\ 2 \\ 3 \\ 4 \end{matrix} & \begin{pmatrix} \sqrt{\frac{2}{13}} & \frac{\sqrt{2}}{2} & 0 & -\frac{1}{2} \\ -\frac{3}{\sqrt{26}} & 0 & -\frac{\sqrt{2}}{2} & -\frac{1}{2} \\ \sqrt{\frac{2}{13}} & -\frac{\sqrt{2}}{2} & 0 & -\frac{1}{2} \\ -\frac{3}{\sqrt{26}} & 0 & \frac{\sqrt{2}}{2} & -\frac{1}{2} \end{pmatrix} \end{matrix} \quad (\text{A8})$$

and related eigenvalues $\lambda = (-\frac{2}{3}, -\frac{1}{3}, 0, 1)$. Each column of \mathbf{g} corresponds to different ω and consecutive rows are node numbers. As mentioned before, $\lambda = 1$ is not taken into account in further calculations, so $\omega = \{\omega_1, \omega_2, \omega_3\} = \{\arccos(-\frac{2}{3}), \arccos(-\frac{1}{3}), \frac{\pi}{2}\}$. Now, having calculated \mathbf{g} and ω we are able to obtain $C(e, \omega)$ and $B(e, \omega)$ as described in Eq. (A3). To simplify the outcome we show it as matrices with rows denoted by graph edges and columns — by ω values:

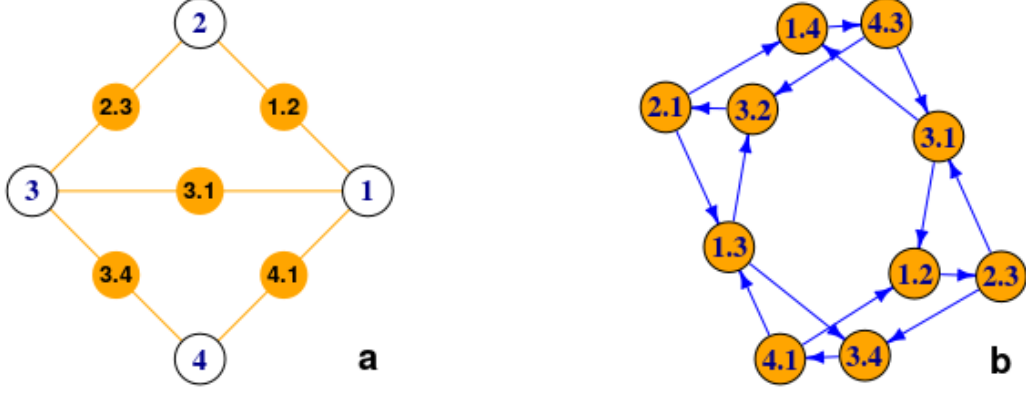


FIG. 10. (a) An example of a simple graph consisting of $|V| = 4$ nodes and $|E| = 5$ edges. (b) Oriented Line Graph obtained from the graph depicted in panel (a).

$$\mathbf{C} = \begin{matrix} & \omega_1 & \omega_2 & \omega_3 \\ \begin{matrix} e_{12} \\ e_{13} \\ e_{14} \\ e_{21} \\ e_{23} \\ e_{31} \\ e_{32} \\ e_{34} \\ e_{41} \\ e_{43} \end{matrix} & \begin{pmatrix} -\frac{3\sqrt{26}}{26} & -\frac{3}{4} & \frac{\sqrt{2}}{2} \\ -\frac{1}{13}\sqrt{6}\sqrt{26} & -\frac{\sqrt{3}}{2} & 0 \\ -\frac{3\sqrt{26}}{26} & -\frac{3}{4} & \frac{\sqrt{2}}{2} \\ \frac{3\sqrt{26}}{26} & \frac{3}{4} & -\frac{\sqrt{2}}{2} \\ \frac{3\sqrt{26}}{26} & \frac{3}{4} & -\frac{\sqrt{2}}{2} \\ -\frac{1}{13}\sqrt{6}\sqrt{26} & \frac{\sqrt{3}}{2} & 0 \\ -\frac{3\sqrt{26}}{26} & \frac{3}{4} & \frac{\sqrt{2}}{2} \\ -\frac{3\sqrt{26}}{26} & \frac{3}{4} & \frac{\sqrt{2}}{2} \\ \frac{3\sqrt{26}}{26} & \frac{3}{4} & \frac{\sqrt{2}}{2} \\ \frac{3\sqrt{26}}{26} & \frac{3}{4} & \frac{\sqrt{2}}{2} \end{pmatrix} \end{matrix}$$

$$\mathbf{B} = \begin{matrix} & \omega_1 & \omega_2 & \omega_3 \\ \begin{matrix} e_{12} \\ e_{13} \\ e_{14} \\ e_{21} \\ e_{23} \\ e_{31} \\ e_{32} \\ e_{34} \\ e_{41} \\ e_{43} \end{matrix} & \begin{pmatrix} \arctan \frac{\sqrt{5}}{2} & -\arctan \frac{\sqrt{2}}{4} & \frac{\pi}{2} \\ -\arctan \sqrt{5} & \arctan \frac{\sqrt{2}}{2} & 0 \\ \arctan \frac{\sqrt{5}}{2} & -\arctan \frac{\sqrt{2}}{4} & -\frac{\pi}{2} \\ 0 & -\frac{\pi}{2} & 0 \\ 0 & \frac{\pi}{2} & 0 \\ -\arctan \sqrt{5} & \arctan \frac{\sqrt{2}}{2} & 0 \\ \arctan \frac{\sqrt{5}}{2} & -\arctan \frac{\sqrt{2}}{4} & \frac{\pi}{2} \\ \arctan \frac{\sqrt{5}}{2} & -\arctan \frac{\sqrt{2}}{4} & -\frac{\pi}{2} \\ 0 & -\frac{\pi}{2} & 0 \\ 0 & \frac{\pi}{2} & 0 \end{pmatrix} \end{matrix} \quad (\text{A9})$$

Each column of matrix \mathbf{C} needs to be divided by a corresponding value of $\rho(\omega)$ given by Eq. (A4), i.e., in the case of the exemplary graph $\rho = \{\frac{15}{13}, \frac{3}{2}, 1\}$. In this way we possess full information needed to evaluate values of u_1 .

Figure 10b presents an Oriented Line Graph obtained from the graph shown in Fig. 10a, its adjacency matrix \mathbf{A}_{olg} being simply

$$\mathbf{A}_{olg} = \begin{matrix} & e_{12} & e_{13} & e_{14} & e_{21} & e_{23} & e_{31} & e_{32} & e_{34} & e_{41} & e_{43} \\ \begin{matrix} e_{12} \\ e_{13} \\ e_{14} \\ e_{21} \\ e_{23} \\ e_{31} \\ e_{32} \\ e_{34} \\ e_{41} \\ e_{43} \end{matrix} & \begin{pmatrix} 0 & 0 & 0 & 0 & 1 & 0 & 0 & 0 & 0 & 0 & 0 \\ 0 & 0 & 0 & 0 & 0 & 0 & 1 & 1 & 0 & 0 & 0 \\ 0 & 0 & 0 & 0 & 0 & 0 & 0 & 0 & 0 & 0 & 1 \\ 0 & 1 & 1 & 0 & 0 & 0 & 0 & 0 & 0 & 0 & 0 \\ 0 & 0 & 0 & 0 & 0 & 1 & 0 & 1 & 0 & 0 & 0 \\ 1 & 0 & 1 & 0 & 0 & 0 & 0 & 0 & 0 & 0 & 0 \\ 0 & 0 & 0 & 1 & 0 & 0 & 0 & 0 & 0 & 0 & 0 \\ 0 & 0 & 0 & 0 & 0 & 0 & 0 & 0 & 1 & 0 & 0 \\ 1 & 1 & 0 & 0 & 0 & 0 & 0 & 0 & 0 & 0 & 0 \\ 0 & 0 & 0 & 0 & 0 & 1 & 1 & 0 & 0 & 0 & 0 \end{pmatrix} \end{matrix} \quad (\text{A10})$$

We deliberately refrain from showing the full matrix \mathbf{g}_{olg} of eigenvectors of \mathbf{A}_{olg} as in our case $|E| - |V| = 1$ so there is exactly one eigenvector corresponding to $\lambda = -1$ namely

$$\mathbf{C}_\pi = \begin{pmatrix} \frac{\sqrt{2}}{4} & 0 & -\frac{\sqrt{2}}{4} & \frac{\sqrt{2}}{4} & -\frac{\sqrt{2}}{4} & 0 & -\frac{\sqrt{2}}{4} & \frac{\sqrt{2}}{4} & -\frac{\sqrt{2}}{4} & \frac{\sqrt{2}}{4} \end{pmatrix} \quad (\text{A11})$$

It is now easy to check that if substitute Eq. (A2) with the calculated matrices \mathbf{C} , \mathbf{B} , ω and \mathbf{C}_π and assume that the wave is initially localised on edge $f = \{1, 2\}$ and $t = 0$, the amplitude $u = 1$ for $e = f = \{1, 2\}$ and $u = 0$ in any other case, as expected. The first 10 steps of propagation can be depicted in Fig. 11 (the wave moves toward $v = 2$), showing both amplitudes on edges (panel a) as well as nodes (panel b).

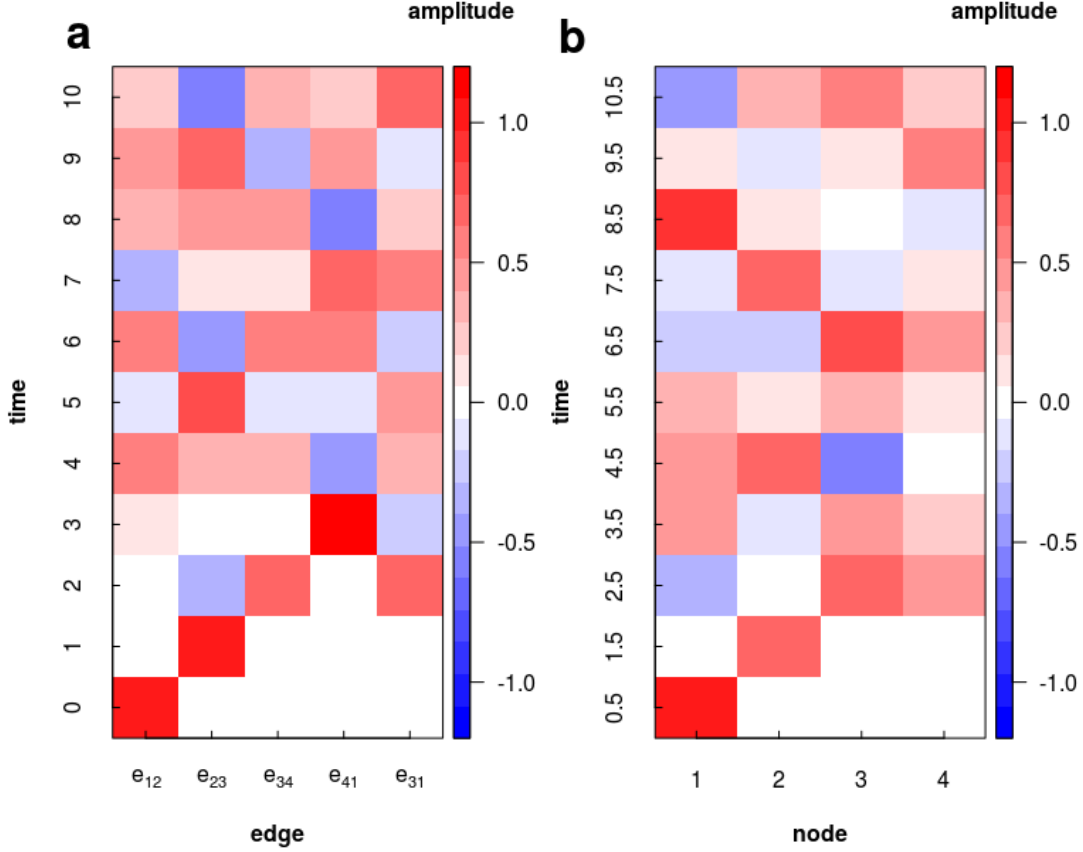


FIG. 11. Wave propagation on a graph shown in Fig. 10a for first 10 time steps (initial condition: a Gaussian wave fully contained on edge $f = \{1, 2\}$ moving toward vertex $v = 2$): (a) amplitudes on edges, (b) amplitudes on nodes.

Appendix B: Principal component analysis

Principal components are a sequence of projections of the set of data in \mathbb{R}^p , mutually uncorrelated and ordered in variance in \mathbb{R}^q where $q \leq p$ [68]. In other words we transform the feature space such that it becomes orthogonal and each consecutive feature is aligned in the direction maximising the variance of the data and has more variance than the last. We do that by minimising the reconstruction error, i.e., solving:

$$\min_{\mathbf{V}_q} \sum_{i=1}^N ||(x_i - \bar{x}) - \mathbf{V}_q \mathbf{V}_q^T (x_i - \bar{x})||^2 \quad (\text{B1})$$

where \mathbf{V}_q is a $p \times q$ matrix with q orthogonal unit vectors as columns. A $p \times p$ matrix $\mathbf{V}_q \mathbf{V}_q^T$ is the *transformation matrix* that maps each p -dimensional observation into its q -rank reconstruction. In our case specifically $p = q = 100$ and the examples of transformation matrices are represented as heat-maps in Fig. 3 and 4. In general PCA is known to be a quick and easy method to (i) perform dimensional reduction, (ii) help to visualise high-dimensional data and (iii) aggregate high-dimensional

data into a possibly single measure (see, e.g., [69–71]).

Appendix C: K-nearest neighbours

In K-NN classification method the class estimation $\hat{y}(x)$ of a given sample x is taken as a majority vote amongst the members of $N_K(x)$ - the neighbourhood of x defined as K points closest to x [68, 72]. To determine which points are closest a metric must be chosen and for the purposes of this paper a Euclidean distance was used. In our case specifically each observation is a graph represented by its WPS, i.e., each graph is a point in a 100-dimensional space.

Appendix D: Fourier analysis

Fourier analysis allows us to convert a given time dependent signal $f(t)$ onto a frequency domain into $\hat{f}(\omega)$ via a Fourier transform and thus acquire the frequency distribution of said signal as it becomes a linear combination of trigonometric functions each corresponding

to a particular frequency. A discrete Fourier transform is as name suggest a discrete version where integration is replaced by summation [73]. Therefore we consider a problem where one wants to express $f(t)$ as a complex Fourier series:

$$\hat{f}(\omega) = \sum_{k=0}^{N-1} f(k) e^{2\pi i \omega / N} \quad (\text{D1})$$

This procedure as it stands would require N^2 operations (where each operation is a complex multiplication followed by a complex addition), however, Cooley and Tukey in [57] presented a method known as the *fast Fourier transform* that allows to do it in less than $2N \log_2 N$.

Appendix E: Real-world networks

We use three real-world networks to test the Fourier transform approach.

Vickers *et al.* [54] collected data from 29 7th grade students from Victoria, Australia. Students were asked to nominate classmates in several categories, three of which were used to construct this 3-layer network. These three categories were determined by questions - Who do you get on with in the class? Who are your best friends in the class? Who would you prefer to work with? The graph has 29 nodes and 740 edges in total.

Krackhardt [58] took a record of relationship between managers in a high-tech company. The graph has 21 nodes and 312 edges in a 3-layer form. Each layer represents a relationship (advice, friendship, "reports to").

Chen *et al.* [59] presented a *Caenorhabditis elegans* multiplex connectome network with 3 layers, 279 nodes and 5863 edges. Each layer corresponds to a different synaptic junction: electric, chemical monadic, and polyadic.

Appendix F: Peak detection using a wavelet transform

A wavelet transform is an analogous procedure to the Fourier transform in the sense that we represent a given signal as an orthonormal series [74]. In case of Fourier those are sine and cosine while in the wavelet those are the eponymous wavelets. A wavelet is a particularly chosen function that is localised, i.e., it has a finite width the its family can compose an orthonormal basis for the signal - $s(t)$.

$$C(a, b) = \int_{\mathcal{R}} s(t) \frac{1}{\sqrt{a}} \psi\left(\frac{t-b}{a}\right) dt, \quad a \in \mathcal{R}^+, b \in \mathcal{R} \quad (\text{F1})$$

In our case the wavelet - ψ - was a Morlet (also known as the Mexican hat) one as per the procedure described in

[60] which (simplified) is as follows: perform a continuous wavelet transform (CWT) on the signal, identify the ridge lines by linking local maxima of CWT at each scale level, identify the peaks based on the ridge lines with three rules (quoted verbatim): "(1) The scale corresponding to the maximum amplitude on the ridge line, which is proportional to the width of the peak, should be within a certain range; (2) The SNR should be larger than a certain threshold; (3) The length of ridge lines should be larger than a certain threshold;". Here SNR is a *signal to noise ratio*.

Appendix G: Exact analytical solutions of wave amplitudes in monoplex and duplex full graphs

1. Monoplex full graph

Here we will consider wave propagation on nodes on a full graph (monoplex) topology, i.e., each node is connected to any other in network, therefore forming a clique of N nodes. In such a case the adjacency matrix \mathbf{A} is a constant matrix filled with ones except for the diagonal which is zero.

It is well known that the spectrum of the full graph consists of $N - 1$ with multiplicity 1 and -1 with multiplicity $N - 1$. As we consider the row-normalised matrix which can be characterised as $\hat{\mathbf{A}} = \frac{1}{N-1} \mathbf{A}$ we have

$$\lambda = \{\lambda_1, \dots, \lambda_{N-1}, \lambda_N\} = \left\{ -\frac{1}{N-1}, \dots, -\frac{1}{N-1}, 1 \right\} \quad (\text{G1})$$

and, consequently, $\omega_i = \arccos\left(-\frac{1}{N-1}\right)$ for $i = 1, \dots, N - 1$. As full graph is $(N - 1)$ -regular then \mathbf{e} , i.e., all-ones vector is an eigenvector of \mathbf{A} corresponding to λ_N while the other vectors can be written as $\mathbf{e}_i - \mathbf{e}_j$ for $i \neq j$, where \mathbf{e}_i is vector with 1 in position i and 0 elsewhere, e.g.,

$$\mathbf{g} = \begin{pmatrix} -1 & -1 & -1 & \dots & -1 & -1 & 1 \\ 0 & 0 & 0 & \dots & 1 & 0 & 1 \\ \vdots & \vdots & \vdots & \ddots & \vdots & \vdots & 1 \\ 0 & 0 & 1 & \dots & 0 & 0 & 1 \\ 0 & 1 & 0 & \dots & 0 & 0 & 1 \\ 1 & 0 & 0 & \dots & 0 & 0 & 1 \end{pmatrix} \quad (\text{G2})$$

After orthonormalising \mathbf{g} with Gram-Schmidt procedure and renumbering the matrix so that the first row becomes the last one we obtain the following $N - 1 \times N$ eigenvector matrix \mathbf{g}_M :

edge e	$C(e, \omega_{N-2})$	$B(e, \omega_{N-2})$	$C(e, \omega_{N-1})$	$B(e, \omega_{N-1})$
e_{12}	$\sqrt{\frac{N-1}{N}}$	$-\frac{\pi}{2}$	$\sqrt{\frac{N-1}{N}}$	0
e_{1k}	$\sqrt{\frac{N-1}{N} \frac{1}{N-2}}$	$\frac{\pi}{2}$	$\sqrt{\frac{N-1}{N}}$	0
e_{21}	$\sqrt{\frac{N-1}{N}}$	$-\arctan\left(\frac{1}{\sqrt{N(N-2)}}\right)$	$-\sqrt{\frac{N-1}{N}}$	$\arctan\left(\sqrt{N(N-2)}\right)$

TABLE I. Coefficients C and B for the full graph case; in the third row $k = 2, \dots, N$.

$$\mathbf{gM} = \begin{pmatrix} 0 & 0 & 0 & 0 & 0 & 0 & 0 & \sqrt{\frac{N-1}{N}} \\ \vdots & \vdots & \vdots & \vdots & \vdots & 0 & \sqrt{\frac{N-2}{N-1}} & -\frac{1}{\sqrt{(N-1)N}} \\ \vdots & \vdots & \vdots & \vdots & 0 & \sqrt{\frac{j}{j+1}} & \dots & \vdots \\ \vdots & \vdots & \vdots & 0 & \dots & -\frac{1}{\sqrt{j(j+1)}} & \dots & \vdots \\ \vdots & \vdots & 0 & \dots & \dots & \vdots & \dots & \vdots \\ \vdots & 0 & \sqrt{\frac{3}{4}} & \dots & \dots & -\frac{1}{\sqrt{j(j+1)}} & \dots & -\frac{1}{\sqrt{(N-1)N}} \\ 0 & \sqrt{\frac{2}{3}} & -\frac{1}{\sqrt{3 \cdot 4}} & \dots & \dots & -\frac{1}{\sqrt{j(j+1)}} & \dots & -\frac{1}{\sqrt{(N-1)N}} \\ \sqrt{\frac{1}{2}} & -\frac{1}{\sqrt{2 \cdot 3}} & -\frac{1}{\sqrt{3 \cdot 4}} & \dots & \dots & -\frac{1}{\sqrt{j(j+1)}} & \dots & -\frac{1}{\sqrt{(N-1)N}} \\ -\frac{1}{\sqrt{1 \cdot 2}} & -\frac{1}{\sqrt{2 \cdot 3}} & -\frac{1}{\sqrt{3 \cdot 4}} & \dots & \dots & -\frac{1}{\sqrt{j(j+1)}} & \dots & -\frac{1}{\sqrt{(N-1)N}} \end{pmatrix} \quad (\text{G3})$$

Note that we deliberately omit the eigenvector corresponding to ω_N which consists of N values $1/\sqrt{N}$ gathered in a column vector

$$\mathbf{C}_M = \left(\frac{1}{\sqrt{N}}, \dots, \frac{1}{\sqrt{N}} \right)^T \quad (\text{G4})$$

as it does not play any role in further calculations.

Let us now assume, that the wave is initially contained on edge $f = e_{uv}$. We are bound to obtain two expressions: one showing the amplitude of the wave at node v which can be simply calculated as $u_n(f, f, t)$ and the other one, showing the sum of the amplitudes for all nodes which can be expressed as

$$u_{all} = u_n(e_{vu}, f, t) + \sum_{i=1, \dots, N, i \neq u} u_n(e_{ui}, f, t). \quad (\text{G5})$$

We will further assume, without losing any generality, that $f = e_{12}$. Such a setting greatly simplifies further calculations of u_n as in this case the only non-zero inputs come from eigenvalues ω_{N-2} and ω_{N-1} . For any other ω_i with $i = 1, \dots, N-3$ we have $C(f, \omega_i) = 0$. Respective coefficients C and B for ω_{N-2} and ω_{N-1} are gathered in Table I

As mentioned in Appendix A, in order to have a proper form of the eigenfunction ϕ one needs to calculate the normalisation factor $\rho(\omega)$. Following we show how to obtain $\rho(\omega_{N-1})$: Eq. (A4) states that it is necessary to sum of over all edges in the networks, however in the case of ω_{N-1} there are only two different terms. The first one ρ_1 comes from $(N-1)$ pairs $e_{12}, e_{13}, \dots, e_{1N}$ the second

one ρ_2 from all the other $\frac{1}{2}(N-1)(N-2)$ pairs, i.e., $e_{23}, \dots, e_{2N}, e_{34}, \dots, e_{N-1N}$ so

$$\rho(\omega_{N-1}) = \sqrt{(N-1)\rho_1 + \frac{1}{2}(N-1)(N-2)\rho_2} \quad (\text{G6})$$

Values of C and B for ρ_1 are shown in Table (I) – taking into account that $B = 0$, the value of ρ_1 simplifies to:

$$\rho_1 = \frac{N-1}{N} \left[\frac{1}{2} + \frac{\sin \left[2 \arccos \left(-\frac{1}{N-1} \right) \right]}{4 \arccos \left(-\frac{1}{N-1} \right)} \right]. \quad (\text{G7})$$

Substituting $\sin(2 \arccos x)$ with $2x\sqrt{1-x^2}$ we arrive at

$$\rho_1 = \frac{N-1}{N} \left[\frac{1}{2} - \frac{2 \frac{\sqrt{N(N-2)}}{(N-1)^2}}{4 \arccos \left(-\frac{1}{N-1} \right)} \right]. \quad (\text{G8})$$

In the case of ρ_2 values C and B can be written as

$$C(e_{ik}, \omega_{N-1}) = -\sqrt{\frac{2}{N(N-2)}} \quad (\text{G9})$$

$$B(e_{ik}, \omega_{N-1}) = -\arctan \sqrt{\frac{N}{N-2}} \quad (\text{G10})$$

for $i = 2, \dots, N-1$ and $k = i+1, \dots, N$ which results in the following form of ρ_2 :

$$\rho_2 = \frac{2}{N(N-2)} \left[\frac{1}{2} + \frac{\sin \left[2 \arccos \left(-\frac{1}{N-1} \right) - 2 \arctan \sqrt{\frac{N}{N-2}} \right] + \sin \left(2 \arctan \sqrt{\frac{N}{N-2}} \right)}{4 \arccos \left(-\frac{1}{N-1} \right)} \right]. \quad (\text{G11})$$

Here, making use of the fact that $\arccos x = 2 \arctan \frac{\sqrt{1-x^2}}{1+x}$ we arrive at

$$\rho_2 = \frac{2}{N(N-2)} \left[\frac{1}{2} + \frac{2 \sqrt{\frac{N(N-2)}{N-1}}}{4 \arccos \left(-\frac{1}{N-1} \right)} \right]. \quad (\text{G12})$$

After substituting Eq. (G6) with ρ_1 and ρ_2 given by Eqs. (G8) and (G12) and performing some short algebra we arrive simply at

$$\rho(\omega_{N-1}) = \sqrt{\frac{N-1}{2}}. \quad (\text{G13})$$

With similar calculations it possible to show that $\rho(\omega_{N-2}) = \rho(\omega_{N-1})$ (in fact, this the case for any ω_i other than ω_N).

We can now use the above calculated values of C , B and ρ to express wave amplitude at nodes of the full graph by the means of Eq. (A6) [note that in order to simplify the equation we use transformation of time $t \rightarrow t + \frac{1}{2}$, thus $t = 0$ means that the wave has arrived at the first node]. We shall start with $u_n(e_{12}, e_{12}, t)$ as the simplest case:

$$\begin{aligned} u_n(e_{12}, e_{12}, t) &= \sum_{i=\{N-2, N-1\}} \frac{C^2(e_{12}, \omega_i)}{2\rho^2(\omega_i)} [\cos(\omega_i t) + \cos((t+2)\omega + 2B(e_{12}, \omega_i))] + \frac{1}{E} \\ &= \frac{1}{2\rho^2(\omega_{N-2})} \frac{N-1}{N} [\cos t\omega_{N-2} + \cos[(t+2)\omega_{N-2} - \pi]] + \\ &+ \frac{1}{2\rho^2(\omega_{N-1})} \frac{N-1}{N} [\cos t\omega_{N-1} + \cos[(t+2)\omega_{N-1}]] + \frac{2}{N(N-1)} \end{aligned} \quad (\text{G14})$$

Making use of Eq. (G13) and the fact that $\cos(x - \pi) = -\cos(x)$ as well as denoting $\omega_{N-2} = \omega_{N-1} = \omega$ we arrive

simply at

$$u_n(e_{12}, e_{12}, t) = \frac{2}{N} \cos(t\omega) + \frac{2}{N(N-1)} \quad (\text{G15})$$

with $\omega = \arccos \left(-\frac{1}{N-1} \right)$. In the same manner one can show that

$$u_n(e_{1k}, e_{12}, t) = \frac{1}{N(N-2)} ((N-3) \cos(t\omega) + (N-1) \cos((t+2)\omega)) + \frac{2}{N(N-1)} \quad (\text{G16})$$

for $k = 3, \dots, N$ and

$$u_n(e_{21}, e_{12}, t) = -\frac{2}{N(N-1)} \left(\cos(t\omega) + \sqrt{N(N-2)} \sin((t+2)\omega) \right) + \frac{2}{N(N-1)} \quad (\text{G17})$$

In this way, Eqs (G15)-(G17) fully determine wave amplitude at every node in the considered monoplex full

graph. They can now be put to Eq. (G5) to show that

$$u_{all}^M(t) = \frac{2}{N-1} \quad (\text{G18})$$

edge e	$C(e, \omega_{N-2})$	$B(e, \omega_{N-2})$	$C(e, \omega_{N-1})$	$B(e, \omega_{N-1})$
e_{12}	$\frac{N}{\sqrt{2(N-1)(N+2)}}$	$\frac{\pi}{2}$	$-\sqrt{\frac{N^2-2}{2(N-1)(N+2)}}$	$-\arctan\left(\frac{1}{N-1}\sqrt{\frac{N-2}{N+2}}\right)$
e_{1k}	$\frac{N}{N-2}\frac{1}{\sqrt{2(N-1)(N+2)}}$	$-\frac{\pi}{2}$	$-\sqrt{\frac{N^2-2}{2(N-1)(N+2)}}$	$-\arctan\left(\frac{1}{N-1}\sqrt{\frac{N-2}{N+2}}\right)$
e_{21}	$-\frac{1}{\sqrt{2(N-1)(N+2)}}$	$-\arctan\left(\frac{2}{\sqrt{N^2-4}}\right)$	$\sqrt{\frac{N^2-2}{2(N-1)(N+2)}}$	$\arctan\left((N+1)\sqrt{\frac{N-2}{N+2}}\right)$

TABLE II. Coefficients C and B for the duplex full graph case; in the third row $k = 2, \dots, N$.

edge e	$C(e, \omega_{2N-3})$	$B(e, \omega_{2N-3})$	$C(e, \omega_{2N-2})$	$B(e, \omega_{2N-2})$	$C(e, \omega_{2N-1})$	$B(e, \omega_{2N-1})$
e_{12}	$\sqrt{\frac{N-2}{2(N-1)}}$	$-\frac{\pi}{2}$	$\sqrt{\frac{(N-1)^2+1}{2N(N-1)}}$	$\arctan\left(\frac{1}{N-1}\right)$	$-\sqrt{\frac{1}{2(N-1)}}$	$-\arctan\left(\sqrt{\frac{1}{(N-1)}}$
e_{1k}	$\sqrt{\frac{1}{2(N-2)(N+1)}}$	$\frac{\pi}{2}$	$\sqrt{\frac{(N-1)^2+1}{2N(N-1)}}$	$\arctan\left(\frac{1}{N-1}\right)$	$-\sqrt{\frac{1}{2(N-1)}}$	$-\arctan\left(\sqrt{\frac{1}{(N-1)}}$
e_{21}	$\sqrt{\frac{N-2}{2(N-1)}}$	0	$-\sqrt{\frac{(N-1)^2+1}{2N(N-1)}}$	$\arctan(N-1)$	$-\sqrt{\frac{1}{2(N-1)}}$	$-\arctan\left(\sqrt{\frac{1}{(N-1)}}$

TABLE III. Coefficients C and B for the duplex full graph case (cntd).

which proves that the sum of node amplitudes is constant for any value of t .

2. Duplex full graph

In this part we consider a full graph duplex, i.e., a network consisting of two cliques (full graphs) of N nodes each connected in such a way that node i from the first clique links with node $i + N$ from the second one ($i = 1, \dots, N$). Assuming that \mathbf{A}_N is a $N \times N$ adjacency matrix of a full graph (as in the previous section) and \mathbf{I}_N is a $N \times N$ identity matrix, we can describe the topology of a full graph duplex with its $2N \times 2N$ adjacency matrix \mathbf{A}_d

$$\mathbf{A}_d = \begin{pmatrix} \mathbf{A}_N & \mathbf{I}_N \\ \mathbf{I}_N & \mathbf{A}_N \end{pmatrix} \quad (\text{G19})$$

Owing to the symmetry of the system (each node has exactly N neighbours - $N - 1$ in the layer it belongs to and one that connects it to the second layer) the row-normalised matrix can be characterised simply as $\hat{\mathbf{A}}_d = \frac{1}{N}\mathbf{A}_d$.

In such a setting we can obtain the following orthonormalised $2N \times 2N$ matrix of eigenvectors for the duplex network

$$\mathbf{g}_D = \frac{1}{\sqrt{2}} \begin{pmatrix} -\mathbf{g}_M & \mathbf{g}_M & \mathbf{C}_M & \mathbf{C}_M \\ \mathbf{g}_M & \mathbf{g}_M & -\mathbf{C}_M & \mathbf{C}_M \end{pmatrix} \quad (\text{G20})$$

where \mathbf{g}_M and \mathbf{C}_M are matrices given by Eqs (G3) and (G4) and a corresponding set of $2N$ eigenvalues is

$$\begin{aligned} \lambda &= \{\lambda_1, \dots, \lambda_{N-1}, \lambda_N, \dots, \lambda_{2N-2}, \lambda_{2N-1}, \lambda_{2N}\} = \\ &= \left\{ -\frac{2}{N}, \dots, -\frac{2}{N}, 0, \dots, 0, \frac{N-2}{N}, 1 \right\} \end{aligned} \quad (\text{G21})$$

and, consequently, $\omega_1 = \dots = \omega_{N-1} = \arccos\left(-\frac{2}{N}\right)$, $\omega_N = \dots = \omega_{2N-2} = \frac{\pi}{2}$, $\omega_{2N-1} = \arccos\left(\frac{N-2}{N}\right)$

As in the previous case we assume that the wave is initially placed on the edge $f = e_{12}$ and our goal is to find wave amplitudes on each of the nodes $1, \dots, N$ as well as the total amplitude on a given layer. Again, the choice of the initial edge is a direct consequence of the structure of \mathbf{g}_D as it restricts the set of eigenvalues needed to calculate u_n to $\omega_{N-2}, \omega_{N-1}, \omega_{2N-3}, \omega_{2N-2}$ and ω_{2N-1} - all others result in $C(f, \omega) = 0$. Values of C and B necessary to compute $u_n(e_{12}, e_{12}, t)$, $u_n(e_{1k}, e_{12}, t)$ for $k = 2, \dots, N$ and $u_n(e_{21}, e_{12}, t)$ obtained from \mathbf{g}_D are summed up in Tables II and III. Following similar calculations as in the monoplex case one can show that the normalisation factor is

$$\begin{aligned} \rho(\omega_{N-2}) &= \rho(\omega_{N-1}) = \rho(\omega_{2N-3}) = \\ &= \rho(\omega_{N-2}) = \rho(\omega_{2N-1}) = \sqrt{\frac{N}{2}} \end{aligned} \quad (\text{G22})$$

Using the above-calculated values of C , B and ρ it is possible to give exact solutions for the amplitude at any node v as

$$u_n(e_{uv}, e_{12}, t) = \frac{1}{N^2} \left[1 + \sum_i (c_i^{uv} \cos \omega_i t + s_i^{uv} \sin \omega_i t) \right] \quad (\text{G23})$$

where

$$\begin{aligned} \omega &= \{\omega_1, \omega_N, \omega_{2N-1}\} \\ &= \left\{ \arccos\left(-\frac{2}{N}\right), \frac{\pi}{2}, \arccos\left(\frac{N-2}{N}\right) \right\} \end{aligned} \quad (\text{G24})$$

and respective coefficients for $u_n(e_{12}, e_{12}, t)$ are given by

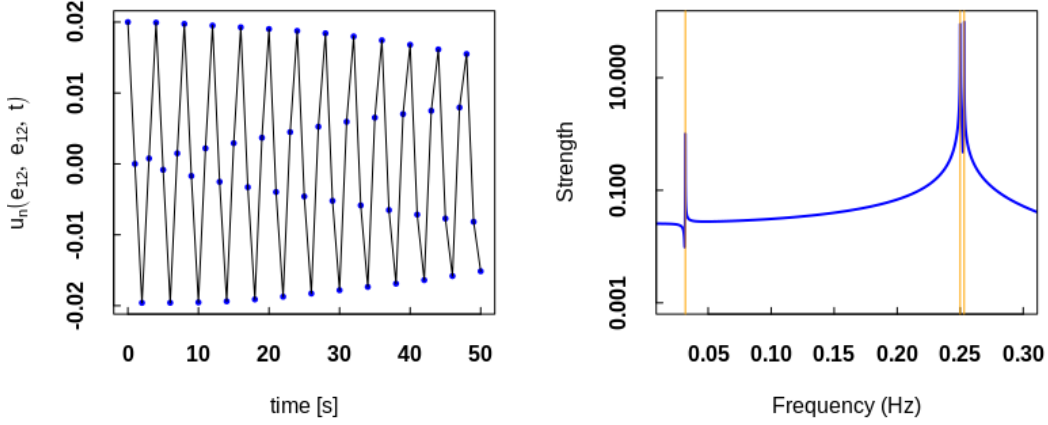


FIG. 12. Full graph duplex with $N = 100$ nodes in each layer: (a) Amplitude at node $v = 2$ over time; lines are guidance to eye connecting theoretical predictions from Eq. (G23) with coefficients \mathbf{c}^{12} and \mathbf{s}^{12} that are exactly covered with points obtained from numerical simulations; (b) Power spectrum of the signal shown in panel (a) [the series consists of 10000 elements]. Vertical lines are drawn for frequencies equal to $\omega_1/2\pi$, $\omega_N/2\pi$ and $\omega_{2N-1}/2\pi$.

$$\mathbf{c}^{12} = \{N - 1, N - 1, 1\} \quad (\text{G25})$$

$$\mathbf{s}^{12} = \left\{ -\sqrt{\frac{N-2}{N+2}}, 1, -\frac{1}{\sqrt{N-1}} \right\}$$

while in the case of $u_n(e_{1k}, e_{12}, t)$, $k = 2, \dots, N$ they are

$$\mathbf{c}^{1k} = \{-1, -1, 1\} \quad (\text{G26})$$

$$\mathbf{s}^{1k} = \left\{ \sqrt{\frac{N+2}{N-2}}, 1, -\frac{1}{\sqrt{N-1}} \right\}$$

and for $u_n(e_{21}, e_{12}, t)$, $k = 2, \dots, N$ we have

$$\mathbf{c}^{21} = \{-1, -1, 1\} \quad (\text{G27})$$

$$\mathbf{s}^{21} = \left\{ -(N+1)\sqrt{\frac{N-2}{N+2}}, -(N-1), -\frac{1}{\sqrt{N-1}} \right\}$$

Finally by calculating

$$u_{all}^D(t) = u_n(e_{12}, e_{12}, t) + (N-2)u_n(e_{1k}, e_{12}, t) + u_n(e_{21}, e_{12}, t) \quad (\text{G28})$$

we arrive at the expression giving the sum of amplitudes over all nodes in a single layer in the duplex full graph which reads

$$u_{all}^D(t) = \frac{1}{N} \left[1 + \cos(t\omega_{2N-1}) - \frac{1}{\sqrt{N-1}} \sin(t\omega_{2N-1}) \right]. \quad (\text{G29})$$

Formula (G23) indicate in the case of single node all three eigenvalues $\arccos(-\frac{2}{N})$, $\frac{\pi}{2}$ and $\arccos(\frac{N-2}{N})$ can be recovered by observing wave amplitude over time at such a node. Indeed the outcomes of the power spectrum shown of numerical implementation of the wave propagation algorithm in Fig. 12 confirm this claim. It should be noted, though, that once N is sufficiently large, two eigenvalues $\arccos(-\frac{2}{N})$ and $\frac{\pi}{2}$ will tend to merge and $\frac{N-2}{N}$ shall approach 1, giving in result two frequencies: $1/4$ and 0 . On the other hand Eq. (G23) clearly shows that if the sum of amplitudes in a single layer is observed then we are able to recover only one eigenvalues, namely $\omega = \arccos(\frac{N-2}{N})$, this fact being depicted in Fig. 9 in the main text.

Appendix H: Amplitude signal on ER graph

As discussed in detail in the main text it is possible to observe oscillations in the known layer induced by the existence of other (unknown) layers. The exact nature of these oscillations depends on the underlying structures of the whole graph and while there is some visible variation on the ER graph as compared to a BA model (see Fig. 13 below and 6 in the main text), similarly to the case of WPS - see Fig. 3 and 4 in the main text - qualitatively these results only further support what can already be seen in Fig. 6, i.e. clear, discernible and consistent peaks in the power spectrum can be detected.

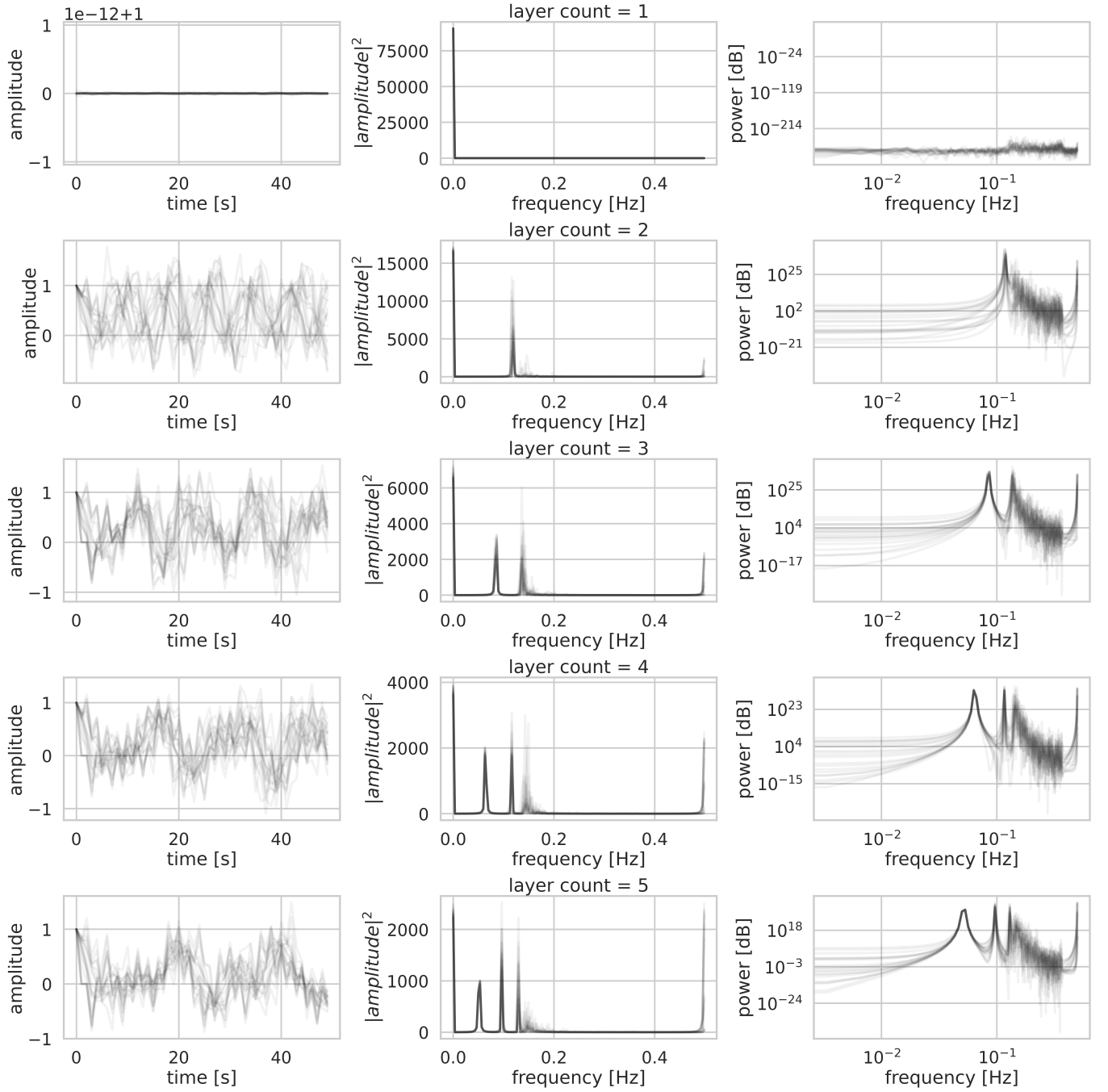


FIG. 13. Sum of amplitudes time evolution as measured on the only visible layer (left). Fast Fourier transform of this signal (centre) and its power spectrum (right). Each row represents a different number of layers (1 to 5 going top to bottom). Simulations conducted on 20 independent realisations of an ER graph ($N = 50$, $\langle k \rangle = 6$) per row, overlaid with transparency. Note: for the purposes of the Fourier analysis we use signals of length 10^3 s.

[1] M. De Domenico, A. Solé-Ribalta, E. Cozzo, M. Kivelä, Y. Moreno, M. A. Porter, S. Gómez, and A. Arenas, Mathematical formulation of multilayer networks, *Physical Review X* **3**, 041022 (2013).

[2] M. De Domenico, C. Granell, M. A. Porter, and A. Arenas, The physics of spreading processes in multilayer networks, *Nature Physics* **12**, 901 (2016).

[3] G. F. de Arruda, F. A. Rodrigues, and Y. Moreno, Fundamentals of spreading processes in single and multilayer

- complex networks, *Physics Reports* **756**, 1 (2018).
- [4] M. Kivelä, A. Arenas, M. Barthelemy, J. P. Gleeson, Y. Moreno, and M. A. Porter, Multilayer networks, *Journal of complex networks* **2**, 203 (2014).
 - [5] S. Boccaletti, G. Bianconi, R. Criado, C. I. Del Genio, J. Gómez-Gardenes, M. Romance, I. Sendina-Nadal, Z. Wang, and M. Zanin, The structure and dynamics of multilayer networks, *Physics Reports* **544**, 1 (2014).
 - [6] A. Barrat, M. Barthelemy, and A. Vespignani, *Dynamical processes on complex networks* (Cambridge university press, 2008).
 - [7] R. Pastor-Satorras, C. Castellano, P. Van Mieghem, and A. Vespignani, Epidemic processes in complex networks, *Reviews of modern physics* **87**, 925 (2015).
 - [8] A. Lokhov, Reconstructing parameters of spreading models from partial observations, in *Advances in Neural Information Processing Systems* (2016) pp. 3467–3475.
 - [9] M. Wilinski and A. Y. Lokhov, Scalable learning of independent cascade dynamics from partial observations, arXiv preprint arXiv:2007.06557 (2020).
 - [10] J. Leskovec and A. Krause, Inferring networks of diffusion and influence, In KDD10 (2010).
 - [11] J. Woo, J. Ok, and Y. Yi, Iterative learning of graph connectivity from partially-observed cascade samples, in *Proceedings of the Twenty-First International Symposium on Theory, Algorithmic Foundations, and Protocol Design for Mobile Networks and Mobile Computing* (2020) pp. 141–150.
 - [12] J. Pouget-Abadie and T. Horel, Inferring graphs from cascades: A sparse recovery framework, in *Proceedings of the 24th International Conference on World Wide Web* (2015) pp. 625–626.
 - [13] B. Abraham, F. Chierichetti, R. Kleinberg, and A. Panconesi, Trace complexity of network inference, in *Proceedings of the 19th ACM SIGKDD international conference on Knowledge discovery and data mining* (2013) pp. 491–499.
 - [14] V. Gripon and M. Rabbat, Reconstructing a graph from path traces, in *2013 IEEE International Symposium on Information Theory* (IEEE, 2013) pp. 2488–2492.
 - [15] M. Gomez-Rodriguez, J. Leskovec, and A. Krause, Inferring networks of diffusion and influence, *ACM Transactions on Knowledge Discovery from Data (TKDD)* **5**, 1 (2012).
 - [16] P. Netrapalli and S. Sanghavi, Learning the graph of epidemic cascades, *ACM SIGMETRICS Performance Evaluation Review* **40**, 211 (2012).
 - [17] A. Braunstein, A. Ingrosso, and A. P. Muntoni, Network reconstruction from infection cascades, *Journal of the Royal Society Interface* **16**, 20180844 (2019).
 - [18] L. Gajewski, K. Suchecki, and J. Hołyst, Multiple propagation paths enhance locating the source of diffusion in complex networks, *Physica A: Statistical Mechanics and its Applications* **519**, 34 (2019).
 - [19] R. Paluch, X. Lu, K. Suchecki, B. K. Szymański, and J. A. Hołyst, Fast and accurate detection of spread source in large complex networks, *Scientific reports* **8**, 1 (2018).
 - [20] R. Paluch, L. G. Gajewski, J. A. Hołyst, and B. K. Szymański, Optimizing sensors placement in complex networks for localization of hidden signal source: A review, *Future Generation Computer Systems* **112**, 1070 (2020).
 - [21] L. Lacasa, I. P. Marino, J. Míguez, V. Nicosia, E. Roldán, A. Lisica, S. W. Grill, and J. Gomez-Gardenes, Multiplex decomposition of non-markovian dynamics and the hidden layer reconstruction problem, *Physical Review X* **8**, 10.1103/physrevx.8.031038 (2018).
 - [22] P. Kuchment, Quantum graphs: I. Some basic structures, *Waves in Random media* **14**, S107 (2004), publisher: Taylor & Francis.
 - [23] P. Kuchment, Quantum graphs: II. Some spectral properties of quantum and combinatorial graphs, *Journal of Physics A: Mathematical and General* **38**, 4887 (2005), publisher: IOP Publishing.
 - [24] P. Kuchment, Quantum graphs: an introduction and a brief survey, arXiv preprint arXiv:0802.3442 (2008).
 - [25] G. Berkolaiko and P. Kuchment, *Introduction to quantum graphs* (American Mathematical Soc., 2013) issue: 186.
 - [26] J. Friedman and J.-P. Tillich, Wave equations for graphs and the edge-based Laplacian, *Pacific Journal of Mathematics* **216**, 229 (2004), publisher: Mathematical Sciences Publishers.
 - [27] N. E. Hurt, *Mathematical physics of quantum wires and devices: From spectral resonances to Anderson localization*, Vol. 506 (Springer Science & Business Media, 2013).
 - [28] L. Pauling, The diamagnetic anisotropy of aromatic molecules, *The Journal of Chemical Physics* **4**, 673 (1936).
 - [29] P. Kuchment, Graph models for waves in thin structures, *Waves in random media* **12**, R1 (2002).
 - [30] J. Biamonte, M. Faccin, and M. De Domenico, Complex networks from classical to quantum, *Communications Physics* **2**, 1 (2019), publisher: Nature Publishing Group.
 - [31] P. Exner and O. Post, Quantum networks modelled by graphs, in *AIP Conference Proceedings*, Vol. 998 (American Institute of Physics, 2008) pp. 1–17.
 - [32] M. Faccin, P. Migdal, T. H. Johnson, V. Bergholm, and J. D. Biamonte, Community detection in quantum complex networks, *Physical Review X* **4**, 041012 (2014), publisher: APS.
 - [33] M. Faccin, T. Johnson, J. Biamonte, S. Kais, and P. Migdal, Degree distribution in quantum walks on complex networks, *Physical Review X* **3**, 041007 (2013), publisher: APS.
 - [34] M. Cuquet and J. Calsamiglia, Entanglement percolation in quantum complex networks, *Physical review letters* **103**, 240503 (2009), publisher: APS.
 - [35] F. Aziz, R. C. Wilson, and E. R. Hancock, A wave packet signature for complex networks, *Journal of Complex Networks* **7**, 346 (2019).
 - [36] V. Kostyrykin, J. Potthoff, and R. Schrader, Finite propagation speed for solutions of the wave equation on metric graphs, *Journal of Functional Analysis* **263**, 1198 (2012), publisher: Elsevier.
 - [37] S. Gomez, A. Diaz-Guilera, J. Gomez-Gardenes, C. J. Perez-Vicente, Y. Moreno, and A. Arenas, Diffusion dynamics on multiplex networks, *Physical review letters* **110**, 028701 (2013).
 - [38] A. Sole-Ribalta, M. De Domenico, N. E. Kouvaris, A. Diaz-Guilera, S. Gomez, and A. Arenas, Spectral properties of the laplacian of multiplex networks, *Physical Review E* **88**, 032807 (2013).
 - [39] F. Aziz, R. C. Wilson, and E. R. Hancock, Analysis of wave packet signature of a graph, in *International Conference on Computer Analysis of Images and Patterns* (Springer, 2013) pp. 128–136.
 - [40] F. Aziz, R. C. Wilson, and E. R. Hancock, Graph characterization using gaussian wave packet signature, in *Inter-*

- national Workshop on Similarity-Based Pattern Recognition* (Springer, 2013) pp. 176–189.
- [41] R. C. Wilson, F. Aziz, and E. R. Hancock, Eigenfunctions of the edge-based laplacian on a graph, *Linear Algebra and its Applications* **438**, 4183 (2013).
 - [42] I. Pesenson, Analysis of band-limited functions on quantum graphs, *Applied and Computational Harmonic Analysis* **21**, 230 (2006), publisher: Elsevier.
 - [43] I. Pesenson, Band limited functions on quantum graphs, *Proceedings of the American Mathematical Society* **133**, 3647 (2005).
 - [44] P. Exner and D. Barseghyan, Spectral analysis of Schrödinger operators with unusual semiclassical behavior, *Acta Polytechnica* **53** (2013).
 - [45] C. Cattaneo, The spectrum of the continuous Laplacian on a graph, *Monatshefte für Mathematik* **124**, 215 (1997), publisher: Springer.
 - [46] M. Kac, Can one hear the shape of a drum?, *The american mathematical monthly* **73**, 1 (1966).
 - [47] C. Gordon, P. Perry, and D. Schueth, Isospectral and isoscattering manifolds: a survey of techniques and examples, *Contemporary Mathematics* **387**, 157 (2005).
 - [48] R. Band, A. Sawicki, and U. Smilansky, Scattering from isospectral quantum graphs, *Journal of Physics A: Mathematical and Theoretical* **43**, 415201 (2010).
 - [49] R. Band, A. Sawicki, and U. Smilansky, Note on the role of symmetry in scattering from isospectral graphs and drums, *Acta Physica Polonica A* **120** (2011).
 - [50] O. Hul, M. Ławniczak, S. Bauch, A. Sawicki, M. Kuś, and L. Sirko, Are scattering properties of graphs uniquely connected to their shapes?, *Phys. Rev. Lett.* **109**, 040402 (2012).
 - [51] U. Smilansky, Delay-time distribution in the scattering of time-narrow wave packets.(i), *Journal of Physics A: Mathematical and Theoretical* **50**, 215301 (2017).
 - [52] U. Smilansky and H. Schanz, Delay-time distribution in the scattering of time-narrow wave packets (ii)—quantum graphs, *Journal of Physics A: Mathematical and Theoretical* **51**, 075302 (2018).
 - [53] M. Robinson, Inverse problems in geometric graphs using internal measurements (2010), arXiv:1008.2933 [math.MG].
 - [54] M. Vickers and S. Chan, Representing classroom social structure, Victoria Institute of Secondary Education, Melbourne (1981).
 - [55] J. Friedman and J.-P. Tillich, Calculus on graphs, arXiv preprint cs/0408028 (2004).
 - [56] U. Brandes, A faster algorithm for betweenness centrality, *Journal of mathematical sociology* **25**, 163 (2001).
 - [57] J. W. Cooley and J. W. Tukey, An algorithm for the machine calculation of complex fourier series, *Mathematics of computation* **19**, 297 (1965).
 - [58] D. Krackhardt, Cognitive social structures, *Social networks* **9**, 109 (1987).
 - [59] B. L. Chen, D. H. Hall, and D. B. Chklovskii, Wiring optimization can relate neuronal structure and function, *Proceedings of the National Academy of Sciences* **103**, 4723 (2006).
 - [60] P. Du, W. A. Kibbe, and S. M. Lin, Improved peak detection in mass spectrum by incorporating continuous wavelet transform-based pattern matching, *Bioinformatics* **22**, 2059 (2006), <https://academic.oup.com/bioinformatics/article-pdf/22/17/2059/767773/btl355.pdf>.
 - [61] M. Chu, M. T. Chu, G. Golub, and G. H. Golub, *Inverse eigenvalue problems: theory, algorithms, and applications*, Vol. 13 (Oxford University Press, 2005).
 - [62] G. Steidl and M. Winkler, A new constrained optimization model for solving the nonsymmetric stochastic inverse eigenvalue problem, arXiv preprint arXiv:2004.07330 (2020).
 - [63] F. Cacace, A. Germani, and C. Manes, Karpelevich theorem and the positive realization of matrices, in *2019 IEEE 58th Conference on Decision and Control (CDC)* (IEEE, 2019) pp. 6074–6079.
 - [64] Z. Zhao, X.-Q. Jin, and Z.-J. Bai, A geometric nonlinear conjugate gradient method for stochastic inverse eigenvalue problems, *SIAM Journal on Numerical Analysis* **54**, 2015 (2016).
 - [65] R. Orsi, Numerical methods for solving inverse eigenvalue problems for nonnegative matrices, *SIAM Journal on Matrix Analysis and Applications* **28**, 190 (2006).
 - [66] R. J. Sánchez-García, E. Cozzo, and Y. Moreno, Dimensionality reduction and spectral properties of multilayer networks, *Physical Review E* **89**, 052815 (2014).
 - [67] E. Cozzo, G. F. de Arruda, F. A. Rodrigues, and Y. Moreno, Multilayer networks: metrics and spectral properties, in *Interconnected Networks* (Springer, 2016) pp. 17–35.
 - [68] T. Hastie, R. Tibshirani, and J. Friedman, *The elements of statistical learning: data mining, inference, and prediction* (Springer Science & Business Media, 2009).
 - [69] L. G. Gajewski, J. Chołoniowski, and J. A. Hołyst, Key Courses of Academic Curriculum Uncovered by Data Mining of Students’ Grades, *Acta Physica Polonica A* **129**, 1071 (2016), arXiv:1604.07074 [physics.ed-ph].
 - [70] J. Sienkiewicz, K. Soja, J. A. Hołyst, and P. M. Słot, Categorical and geographical separation in science, *Scientific reports* **8**, 1 (2018).
 - [71] J. Chołoniowski, J. Sienkiewicz, N. Dretnik, G. Leban, M. Thelwall, and J. A. Hołyst, A calibrated measure to compare fluctuations of different entities across timescales, *Scientific Reports* **10**, 20673 (2020).
 - [72] T. Cover and P. Hart, Nearest neighbor pattern classification, *IEEE transactions on information theory* **13**, 21 (1967).
 - [73] G. B. Arfken and H. J. Weber, *Mathematical methods for physicists* (1999).
 - [74] I. Daubechies, *Ten lectures on wavelets* (SIAM, 1992).